Rancho Seco Non-Industrial Area Survey Project

Final Report, Revision 2

June 26, 2001

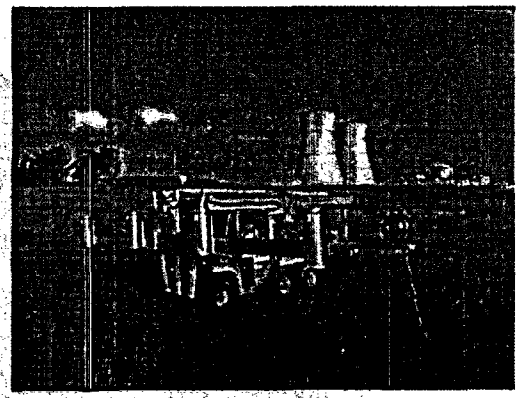

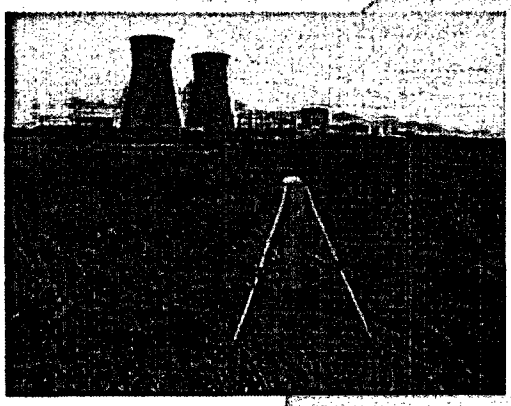

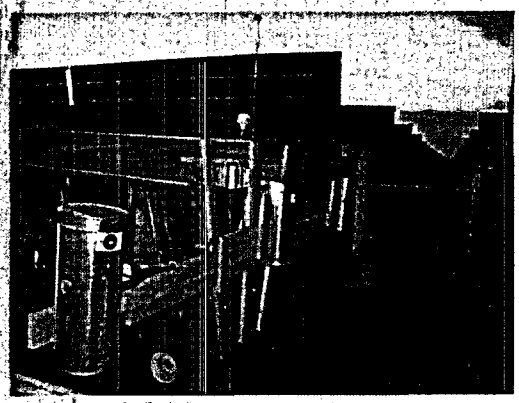

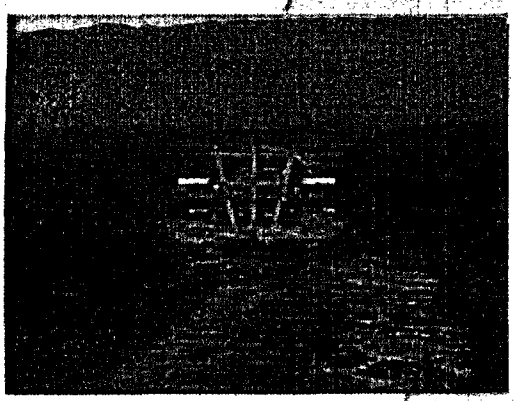

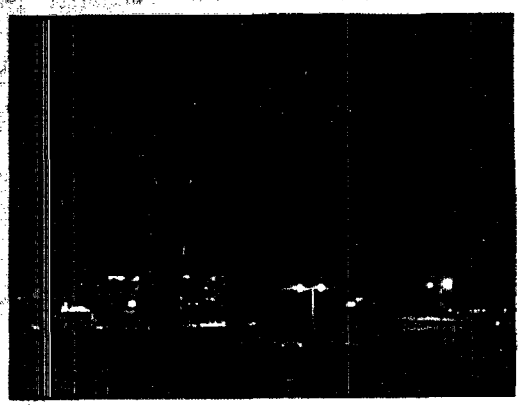

Shonka Research Associates, Inc.
4939 Lower Roswell Road
Suite 106
Marietta GA 30068
(770) 509-7606

Volume I

Table of Contents

VOLUME I – Discussion of Methods and Results

1. Introduction

Rancho Seco Nuclear Generating Station is a non-operating 913 MW Pressurized Water Reactor owned by the Sacramento Municipal Utility District (the District). Rancho Seco, located about 25 miles south of Sacramento, operated from April 1975 to June 1989, but was closed by public referendum. It is currently in full-plant decommissioning and dismantlement.

The District solicited proposals for the performance of Radiological Surveys and evaluations of designated areas of the site outside the Industrial Area of the Rancho Seco Nuclear Station to support a report to the Nuclear Regulatory Commission (NRC) to determine the boundary of any impacted areas as well background survey values for comparison to impacted area values. Shonka Research Associates, Inc. (SRA) was awarded the contract to design and perform the surveys. The purpose of the survey, as conveyed by the District, is to support consideration of placement of a proposed gas-fired plant on the Rancho Seco site, to the south of the industrial area where the nuclear plant is located.

Highlights of the survey include:

- 100% scan of 76 acres (308,000 m^2) of land within the Rancho Seco Owner Controlled Area were surveyed in less than 3 weeks time;
- All survey areas were verified to be non-impacted with no contamination in excess of background detected (See Appendix H);
- Over 80,000 gamma spectra were collected and processed during the survey project;
- Achievement of sensitivities between one and two orders of magnitude less than the Derived Concentration Guidelines stated in the Request for Proposal No. 0332-JHB;
- Completed performance tests consisting of repeated grids, grids "salted" with check sources, and a grid intentionally placed in a known contaminated effluent area. These tests verified the capabilities of the systems deployed to Rancho Seco at no additional cost to SMUD (see Appendix I);
- Additional measurements were also made inside of the industrial area to provide information about radiological conditions in the vicinity of the Independent Spent Fuel Storage Installation (ISFSI), prior to its loading with spent reactor fuel.

Twelve areas were selected to survey the plant, including areas that bounded the plant or were potentially impacted, and areas well outside of the industrial center of the site. The bounding areas were surveyed with more than 50% of the area scanned with the area chosen in a checkerboard fashion. Areas well outside of the industrial center of the site were scanned with 10% coverage.

Excluded from the survey domain were the balance of the industrial area itself, as well as the parking lots located to the east of the plant. The parking lots continue to be used for staging shipments of radioactive waste, and remain an area of the site needed to support decommissioning. Also excluded from the survey domain was the pathway for normal effluents, located to the southwest of the industrial area. This pathway for liquid effluents contains known and well-characterized residual radioactivity from the plant in excess of background. In addition, the area immediately to the west of the industrial area has been excluded since it has been designated for the ISFSI.

The surveys were performed by Shonka Research Associates, Inc. (SRA), using advanced technologies developed by SRA. Scan surveys were performed with the Subsurface Multi-Spectral Contamination Monitor (SMCM) as well as traditional measurements with fixed Sodium Iodide (NaI(Tl)) detectors. Additionally, soil samples were collected by SRA at specific points identified during the survey and analyzed by Rancho Seco personnel.

The survey team consisted of Dr. Joseph Shonka, Mr. Don Debord, Mr. Joe Weismann, and Mr. Richard Turner of Shonka Research Associates, Inc.

2. Methodology

2.1 Establishment of Survey Areas

To achieve the survey goals introduced in Section 1, the areas were split into two discrete categories:

- Areas requiring 10% areal scan survey (non-impacted), and
- Areas requiring 50% areal scan survey (bounding and potentially impacted areas).

Based on this requirement and guidance from the Rancho Seco Staff, the following Survey Areas were defined as shown in Table 2-1:

Table 2-1 - Survey Areas

Survey Area	Survey Requirement
A – Gas-Fired Plant	10%
B - Effluents	50%
C - Outfalls South	Split (50% & 10%)
D - Outfalls North	Split (50% & 10%)
E - Westside	10%
F - Northwest Side	10%
G - PV Plant – Outside	10%
H - Parking Lot	10%
I - PV Plant - Inside	10%
J - Roads	N/A
K - Industrial Area	N/A
M – ISFSI	N/A

The alphabetical designation refers to the relative priority of the Survey Area as determined by Rancho Seco staff. The "N/A" designation means that no preset survey area requirement was stated for these areas. The extent of the survey performed would be decided by the SRA field team and Rancho Seco staff. The physical location boundaries of these Survey Areas are shown in Figure 2-1 superimposed on an aerial photograph of the Rancho Seco site.

Figure 2-1 - Defined Survey Areas.

2.1.1 Placement of Survey Area Blocks

Using the information provided in Table 2-1, the Survey Areas were investigated for placement of Survey Area Blocks (SABs). A SAB is defined as an area inside which 100% of the area is surveyed. Based on the land area requiring survey and the capabilities of the SMCM, SRA chose a SAB size of 100 meters by 48 meters for the scan surveys. Therefore, approximately 60 SABs were required to satisfy the areal criteria defined in Section 2 of the RFP. The 50% areas were

C01

covered using a "checkerboard" design as this was viewed as the approach most likely to identify streaming contamination patterns through the SAB. SABs in the 10% areas were placed in random locations as a means for providing a representative sampling of the entire area. The Outfalls South (C) and Outfalls North (D) areas had to be subdivided to achieve the 50% areal coverage requirements outlined. The Effluents Area (B) was split into two survey areas, each with 50% coverage outlined.

Once the preliminary locations were agreed to by Rancho Seco, latitude and longitude coordinates were obtained for each SAB via Geographical Information System (GIS) software used by SRA for this survey. The southwest corner of each SAB was chosen as the reference point or "monument". Upon arrival at Rancho Seco, members of the SRA field team located the coordinates of each monument through use of a differentially-corrected global positioning system (GPS). Each monument location was marked with a 10 inch iron pin that was driven into the ground. A temporary wooden stake was also driven to help the survey team locate the southwest corner of each SAB. Once the pin was located, a walkdown of the area was performed to ensure that the local terrain would support a rolling survey of 100 meters by 48 meters. If permanent obstacles were encountered, the scan team would attempt to correct the situation in one of two ways; (a) move the SAB away from the obstacle such that a complete, unobstructed scan could be performed, or (b) perform the scan in the SABs original location while navigating around the obstacle. In this case, the survey data will have a "hole" where the obstacle was present. There were a few instances where both approaches had to be taken due to severe obstacles. The "C1000 – Outfalls South" region proved difficult to navigate due to standing water and marshy conditions in its low lying areas. Therefore, the final locations of the SABs are considerably different from those proposed in the Rancho Seco Survey Plan. The completed SAB layout is shown in Figure 2-2. A complete location reference table for all SABs shown in Figure 2-2 can be found in Appendix A.

An artifact in Figure 2-2 is the rotation of some of the SABs relative to the site boundary. The rotated grids were aligned to magnetic north, which is 14.5° east of grid north for the Sacramento area. Midway through the survey effort, the remaining SABs were aligned to grid north.

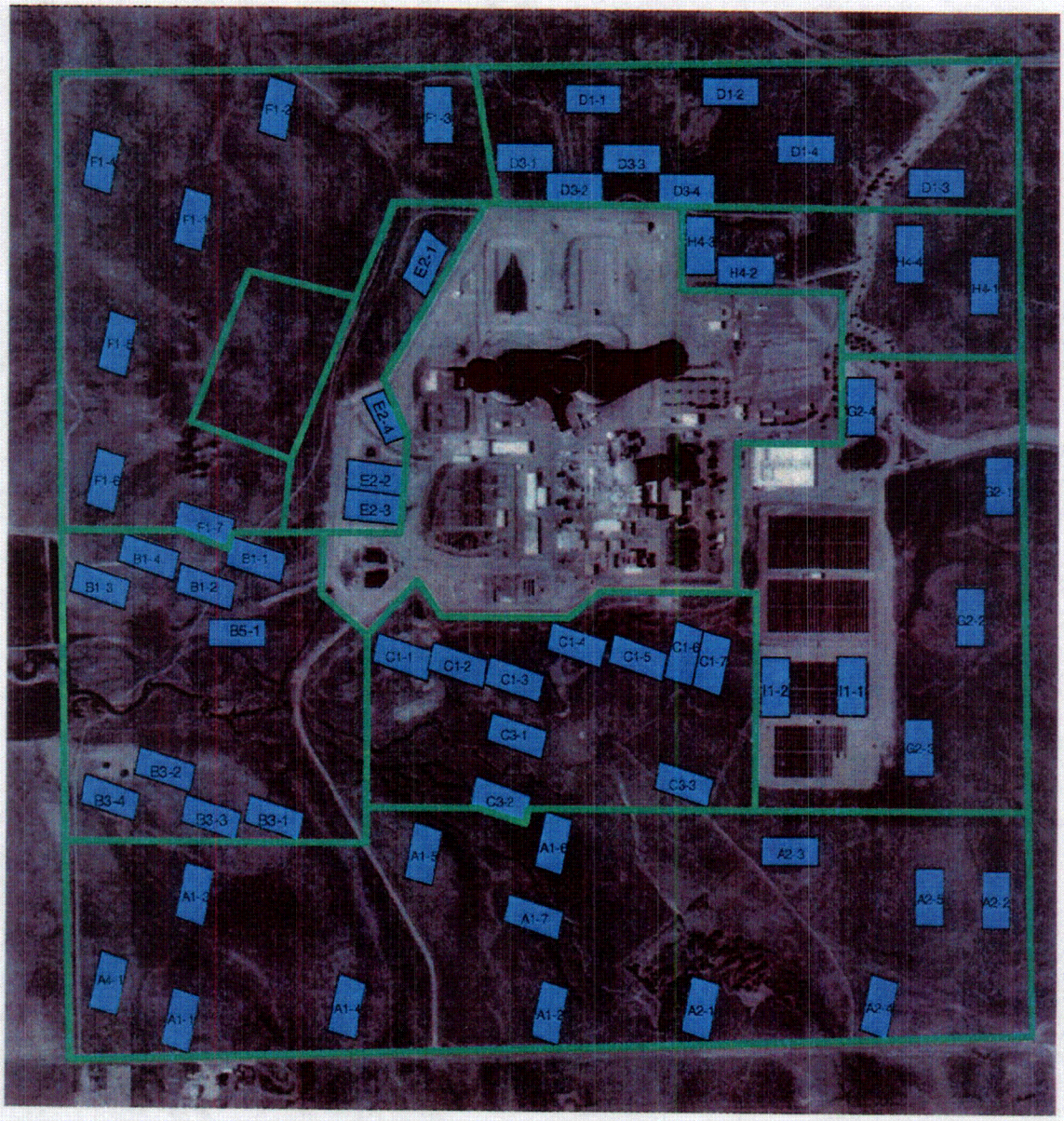

Figure 2-2 – Defined Survey Area Blocks (SABs)

2.1.2 In situ Measurement Locations

For the most part, the *in situ* measurements were taken at the pin location for each SAB. However, there were fifteen SABs that required decoupling of the *in situ* measurement due to obstacles or terrain difficulties encountered by the scan team. A list of these affected SABs is shown in Table 2-2.

Table 2-2 - In situ measurements not taken at pin location.

SAB	Latitude		Longitude		Notes
	Deg	Min	Deg	Min	
Area A - Gas-Fired					
A1000-0003	38	20.292	121	7.775	In situ measurement taken at NE corner of SAB.
Area A - Gas-Fired, East					
A2000-0001	38	20.174	121	7.175	SAB re-located due to terrian restrictions
A2000-0004	38	20.176	121	6.982	SAB re-located due to terrian restrictions
Area C - Outfalls South					
C1000-0002	38	20.556	121	7.481	In situ placed in storm drain outfall flow path. Location marked as C1-LMK026
C1000-0003	38	20.545	121	7.409	In situ placed in storm drain outfall flow path. Location marked as C1-LMK025
C1000-0004	38	20.546	121	7.308	In situ placed in storm drain outfall flow path. Location marked as C1-LMK023a
C1000-0005	38	20.549	121	7.308	In situ placed in storm drain outfall flow path. Location marked as C1-LMK023
C1000-0006	38	20.554	121	7.308	In situ placed in storm drain outfall flow path in close proximity to SAB.
C1000-0007	38	20.556	121	7.308	In situ placed in storm drain outfall flow path. Location marked as C1-LMK027
C3000-0008	38	20.427	121	7.211	In situ measurement taken at NW corner.
Area D - Outfalls North					
D1000-0001	38	21.013	121	7.311	SAB re-located due to terrian restrictions
Area F - Northwest Side					
F1000-0005	38	20.782	121	7.830	SAB re-loacted 37 meters east to avoid obstacle.
F1000-0006	38	20.662	121	7.845	SAB re-loacted 37 meters east to avoid obstacle.
Area H - Parking Lot					
H4000-0002	38	20.844	121	7.139	SAB re-located due to terrian restrictions
H4000-0003	38	20.870	121	7.171	SAB re-located due to terrian restrictions

The C1000 Survey Area was unique in that the *in situ* locations were selected independent of SAB location. The field team decided to take this approach for several reasons: (1) layout of the C1000 SABs in their original locations was impossible due to standing water and muddy areas, and (2) Rancho Seco staff had voiced concern that the C1000 region may be impacted due to potential activity in the storm drain outfalls. For these reasons, new *in situ* measurement locations were selected along the Industrial Area south fence such that the detector would have the greatest probability of detecting residual activity from potential releases. The preferred location was in the base of a gully (or trench) in the flow path of a storm drain outfall. The locations selected are shown in Figure 2-3.

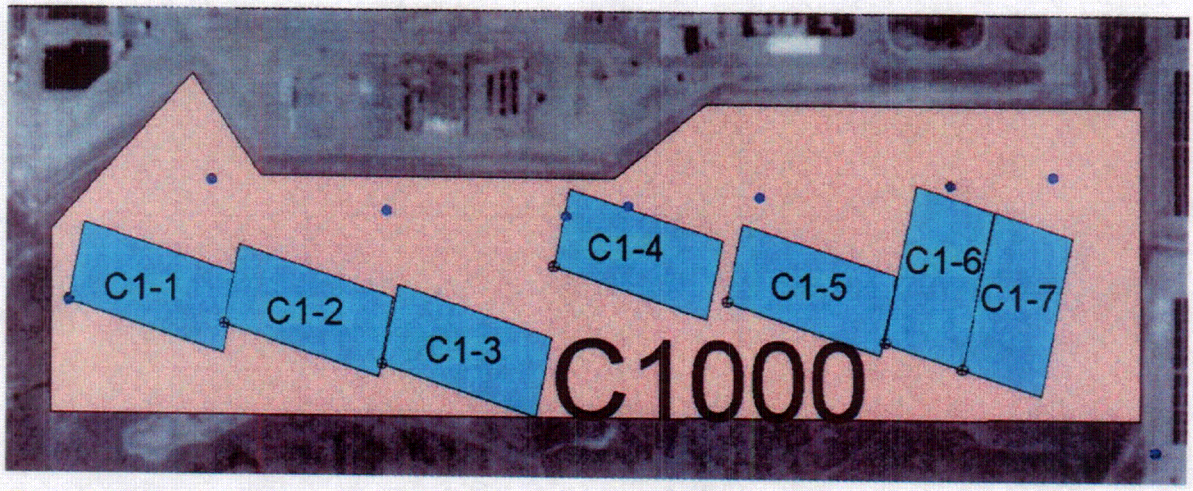

Figure 2-3 – In situ locations for the C1000 Survey Area, shown as the blue dots closest to the Industrial Area fence.

2.1.3 Soil Sample Locations

Each soil sample was taken in close proximity (within 1 meter) to the pin location at the selected SAB. One soil sample was collected for every 2 SABs within a given Survey Area, i.e. C1000, such that a fair representation of the soil in that area was accounted for. The survey maps generated by SRA display soil sample locations with an "X" shaped symbol inside the monument dot. Figure 2-3 shows a close-up of the C1000 Survey Area, with all relevant survey information included.

2.2 Survey Methods

2.2.1 SMCM Scan Surveys

Scan surveys were conducted using the Subsurface Multi-Spectral Contamination Monitor (SMCM) system developed by SRA. The SMCM, as configured for the Rancho Seco survey, consisted of four sodium iodide (NaI(Tl)) gamma scintillators, of nominal size 5 inch by 2 inch right circular cylinder, packaged in heated enclosures for environmental stabilization. The scintillators were placed two meters apart and with the front face of the detector at one meter above the ground in a vertical orientation. The detector enclosures were also equipped with a thin layer of lead shielding for Compton background suppression. The detectors and electronics were mounted to a John Deere™ "Gator" all-terrain utility vehicle and powered using a portable generator. Figure 2-4 shows the SMCM as deployed at Rancho Seco.

Figure 2-4: SRA's SMCM platform as deployed at Rancho Seco.

NaI(Tl) spectra were collected during each 10 second interval while the SMCM traveled 2 meters. This data was then assigned to the center of the 2-meter by 2-meter square under each detector. The MCAs were operated using a field industrial personal computer (PC). The spectra were collected into 512 channels corresponding to a 0.3 to 3 MeV energy range. The energy range includes important photons from primordial nuclides series including potassium (K), uranium (U), and thorium (Th). ("KUT" which are present in parts per million (ppm) levels in most soils.) Each SAB consisted of a nominal 100 meter by 48 meter area, resulting in twenty-four adjacent strips of 100 meters in length being characterized, or 1200 spectral measurements. SAB areas had to be adjusted in some areas where permanent obstacles were present. In these cases, the position and/or size of the SAB was adjusted by the field team to accommodate the available space.

Performance characteristics of the SMCM scan survey platform are discussed in Appendix F.

2.2.2 Data Handling and Analysis Techniques

The data from the SMCM for a given SAB consisted of 1200 each, 10-second spectra from the nominal 5X2 NaI(Tl) detectors. The energy range from 0.3 to 3 MeV was spanned with 512 channels. The data was converted to count rate, and adjusted by a factor that included the detector efficiency (relative to detector #1) and the platform shielding. Following correction of the raw data by the platform-shielding factor, the spectra were analyzed and separated into components using the method of noise-adjusted single value decomposition (NASVD). (Hovgaard 1997) This is a statistical process that computes the spectral shapes that are embedded data. For a more detailed presentation of these data handling and analysis techniques, see Appendix G of this report.

2.2.3 In situ Measurements

Fixed point *in situ* measurements were taken at each SAB location to aid in the overall radiological characterization. A total of 62 *in situ* measurements were taken. SRA's *in situ* system consisted of a NaI(Tl) detector and electronics enclosed in a free-in-air tripod geometry at a fixed height of one meter above the ground, measured from the detector face. The detector was a 3-inch by 3-inch NaI(Tl) Bicron model 3M3/3, serial number AA-4631-I , coupled to an EG&G ORTEC model 296 ScintiPak solid-state tube base, S.N. 707. The Scintipack is equipped with integral high voltage power supplies and preamplifier stage in each unit. An ORTEC MicroNOMAD portable MCA, serial number 355, provided the amplifier stage and the analog-to-digital conversion. Figure 2-5 provides a photograph of SRA's *in situ* system as deployed at Rancho Seco. The MicroNOMAD portable MCA is shown at the base of the wooden stake.

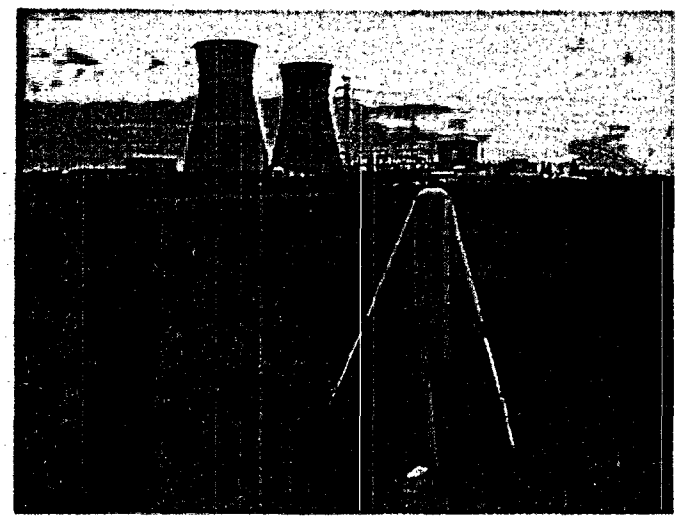

Figure 2-5 - Photograph of SRA's in situ system in use at Rancho Seco.

Each *in situ* measurement was 10 minutes in length. Spectra were collected in the field by the portable MCA and transferred to a laptop computer for processing.

2.2.4 Soil Samples

The samples were collected and labeled by SRA staff in accordance with Rancho Seco procedures. Rancho Seco staff analyzed the samples as taken (wet) and again after drying in a laboratory oven to remove the moisture content.

3. Survey Results

3.1 Scan Surveys

3.1.1 SMCM Results Review

Over 80,000 gamma ray spectra were collected throughout the course of the Rancho Seco Non-Industrial Radiological Survey Project. Each SAB was reviewed for the presence of ^{134}Cs, ^{137}Cs, and ^{60}Co using the methods described in Section 2.2.2 after electronic submittal from the field. No evidence of these nuclides was found. A complete listing of results from the scan survey can be found in Volume II, SMCM Data Tables.

There is an extremely low level of fallout ^{137}Cs present in a largely uniform fashion across the site. The ^{137}Cs is "visible" as a slight broadening of the 609 keV Bi-214 peak that comes from the decay of uranium in the ground and radon in the air. Because it is similar across the site, and below the detection limit of the method, it was not seen as a separate component.

The ^{40}K levels across the Rancho Seco site vary considerably. Results for all completed SABs as images overlaid on the same photograph are shown in Figure 3-1. The SAB images have not been rotated to their correct site orientation. Despite the lack of rotation, the absolute position of the southwest corner (pin location) is still correct. All images have been scaled to the same colormap to show the variability in background levels throughout the site.

SAB G2-4 is particularly interesting as half of the area surveyed was over an abandoned parking lot (yellow), compared to grass in the other half (orange). The aggregate materials used in paving materials are known to have much higher concentrations of ^{40}K as this image shows. The blue areas reflect non-surveyed areas.

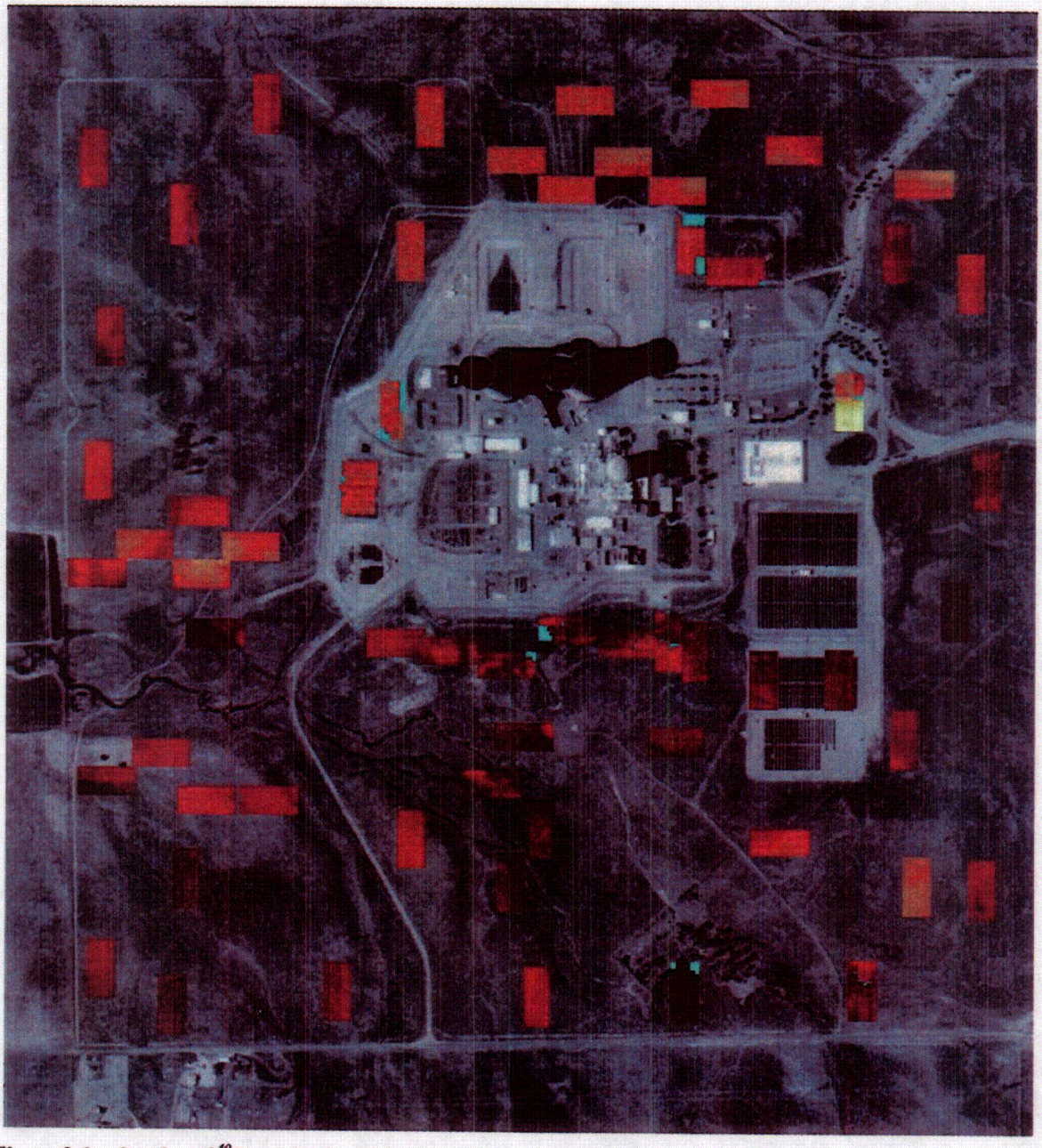

Figure 3-1 – Overlay of ^{40}K results for all SABs. The SABs are not rotated due to limitations of the GIS system.

3.1.2 SMCM Detection Limits

Minimum detectable concentrations (MDCs, in terms of pCi/g for uniformly-distributed material) were computed *a posteriori* for each SAB. The MDC was determined by taking the standard deviation of the 1200 measurements in each SAB and multiplying it by 4.65 to arrive at a 95%-confidence level. The MDC data for the 62 SABs are provided in Volume II of this report. In the case of ^{40}K, the actual mean SAB concentration in pCi/g is reported.

3.1.3 SMCM Quality Control

A discussion of the SMCM Quality Control (QC) procedures and results, including detector control charts, may be found in Appendix B, Detector Quality Control.

3.2 In situ Measurements

3.2.1 Results of in situ Counts

Sixty *in situ* measurements were performed at Rancho Seco during the extent of the survey deployment. The gamma spectra from each of these counts was investigated for positive indication of ^{137}Cs, ^{60}Co, and ^{134}Cs using discrete energy windows surrounding each nuclide's peak location. No evidence of these nuclides was found. Each of the 60 *in situ* spectra may be found in the SAB Radiological Survey Reports, found in Volume II of this report. Table 3-1 provides a summary of the energy windows used.

Table 3-1 – Summary of in situ energy windows for data analysis.

Nuclide	Peak Location (keV)	Energy Window (keV)
^{137}Cs	661.65	610 – 710
^{60}Co	1173.2	1025 – 1250
^{134}Cs	795.8	750 – 840

In the case of ^{134}Cs, which has several prominent photopeaks, the 795.8 keV peak (85.4%) was chosen as it was free of interference by nearby primordial nuclides. For example, ^{134}Cs's 604.7 keV peak has an intensity of 97.6%, but at very low count rates, the 609 keV peak from Bi-214 (Uranium series) would mask any potential to identify it. For similar reasons, only the 1173.2 keV peak for ^{60}Co was used as its 1332.5 keV peak could be biased by interference from ^{40}K at 1461 keV.

3.2.2 In situ Detection Limits

Minimum detectable concentrations (MDCs, in terms of pCi/g for uniformly-distributed material) for the 10-minute counts were computed for each SAB individually. The MDC was determined by integrating the gross counts in the appropriate energy region for each of the 60 spectra acquired. The standard deviation associated with each value was then computed by taking its square-root. These data were divided by 10 minutes to convert to a count rate and then

multiplied by 4.65 to get a 95%-confidence MDC in terms of count rate. (Currie 1968) Finally, the count rates were converted to pCi/g by dividing by the appropriate calibration factor (See Appendix E for details regarding the calibration factors). Detailed MDC data for the 62 SABs are given in Volume II of this report. The computed MDCs are a factor of 10 lower than the Rancho Seco RFP DCGL requirements for ^{137}Cs (5.5 pCi/g), ^{60}Co (1.9 pCi/g), and ^{134}Cs (2.85 pCi/g), which all correspond to 50% of the DCGL screening levels provided in the Federal Register (64 CFR 68395, December 7,1999).

3.2.3 In situ Quality Control

A discussion of the *in situ* QC results, including detector control charts, may be found in Appendix B, Detector Quality Control.

3.3 Soil Sample Results

SRA collected 31 screened, 1-liter soil samples throughout the Rancho Seco Owner Controlled Area. A summary of the wet and dry analysis results is provided in Volume II of this report.

The soil sample results provided in Volume II were compared to the static and scanning *in situ* measurements to gauge their accuracy. For these comparisons, ^{40}K was used as it was the only nuclide that was positively reported by all three platforms. Only the "wet" soil sample results were used in these comparisons as it more accurately reflects the soil condition that the static and rolling platforms were observing during their measurements. The direct comparisons are shown as scatter plots (Figure 3-2 and Figure 3-3) with points representing the measured values at each SAB measurement location. Only those SABs with soil samples are plotted. The boundary lines are ±1-sigma about the "best fit" line. Twenty-nine soil sample results were used in this comparison. Two points were rejected for the following reasons: the first soil sample at SAB B1-2 did not have a corresponding *in situ* count performed; and SAB E2-2 was rejected for the *in situ* comparison with the soil data due to extremely low background in the *in situ* count.

What one would expect from normally distributed data sets is 68% of the points to fall within the ±1-sigma lines, or approximately 20 of the 29 in this data set. For the combined *in situ* and soil data, 23 SAB measurements fall within the ±1-sigma boundaries when accounting for the measurement uncertainties (Figure 3-2). The SMCM scanning measurements (shown in Figure 3-3) also agree with the soil sample results, with 24 measurements falling within 1-sigma boundaries.

The conversion factor for ^{40}K is 0.65 cps per pCi/g due to low abundance and gamma branching ratio. The conversion factor for ^{137}Cs is 7.29 cps per pCi/g. If ^{137}Cs were present and measured by both systems (as was ^{40}K), the scale for corresponding plots would be a factor of 11.2 lower. These comparisons also show good agreement between the SMCM, the static *in situ* counts, and the soil sample results.

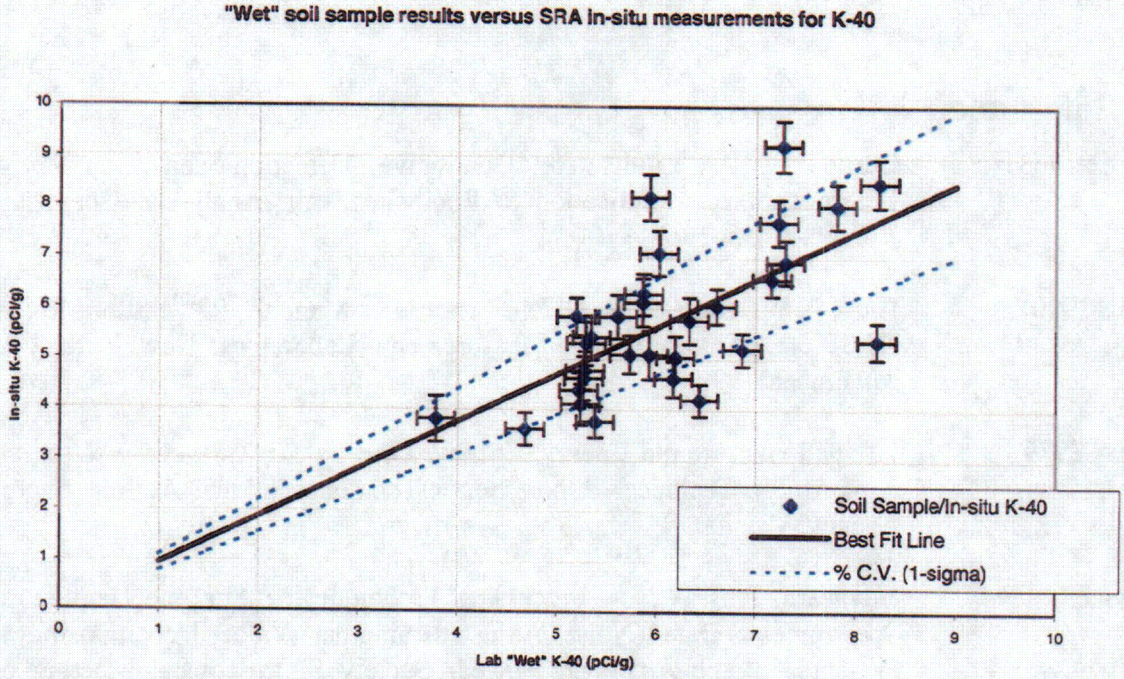

Figure 3-2 - Scatter plot of in situ counts versus lab soil sample results for ^{40}K.

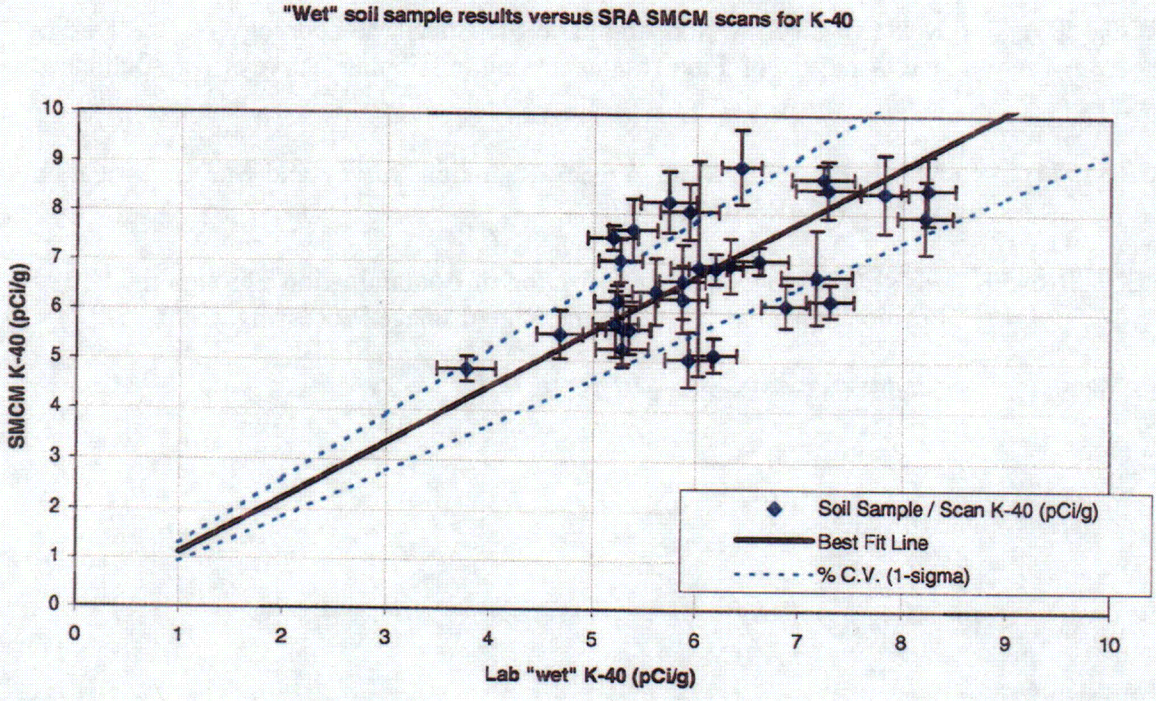

Figure 3-3 - Scatter plot of SMCM scan measurements versus lab soil sample results for ^{40}K.

4. References

(Currie 1968) Currie, L. A. Limits for Qualitative Detection and Quantitative Determination – Application to Radiochemistry. Analytical Chemistry, Vol. 40, No. 3. 1968.

(EML 1990) Krey, P. W.; Beck, H. L. "EML Procedures Manual", 27th edition, Vol. 1, HASL-300, Environmental Measurements Laboratory, New York, NY, November, 1990.

(IAEA 1979) International Atomic Energy Agency. *Gamma Ray Surveys in Uranium Exploration.* Technical Report Series 186. International Atomic Energy Agency, Vienna.

(Hovgaard 1997) Hovgaard, Jens. A New Processing Technique for Airborne Gamma-ray Spectrometer Data (Noise Adjusted Singular Value Decomposition). Presented at the American Nuclear Society Sixth Topical Meeting on Emergency Preparedness and Response, San Francisco, California, April 22-25, 1997.

(NUREG-1505) NUREG-1505, A Nonparametric Statistical Methodology for the Design and Analysis of Final Status Decommissioning Surveys (pre-published report).

(NUREG-1575) NUREG – 1575, Multi-Agency Radiation Survey and Site Investigation Manual (MARSSIM). 1997.

(NUREG/CR-6450) NUREG/CR-6450, Characterization of Contamination Through the Use of Position Sensitive Detectors and Digital Image Processing. 1996.

(64CFR 68395) 64CFR 68395. December 7,1999.

Appendix A

SAB Location Reference Table

SAB	From Reactor		Latitude		Longitude		UTM Easting	UTM Northing	Notes
	Distance	Bearing	degrees	minutes	degrees	minutes			
A1000-0001	1223	227	38	20.180	121	7.793	663445	4244787	
A1000-0002	847	193	38	20.183	121	7.364	664070	4244805	
A1000-0003	1062	233	38	20.292	121	7.775	663467	4244996	
A1000-0004	1000	216	38	20.190	121	7.600	663726	4244811	
A1000-0005	731	216	38	20.326	121	7.509	663854	4245065	
A1000-0006	605	197	38	20.334	121	7.357	664075	4245085	
A1000-0007	701	200	38	20.285	121	7.394	664023	4244993	
A2000-0001	930	173	38	20.185	121	7.189	664325	4244815	SW corner of scan survey. Moved due to terrain
	948	173	38	20.174	121	7.175	664346	4244795	Location of *in situ* count
A2000-0002	953	135	38	20.272	121	6.040	664830	4244967	
A2000-0003	632	156	38	20.333	121	7.093	664459	4245091	
A2000-0004	1004	152	38	20.184	121	6.982	664627	4244819	SW corner of scan survey. Moved due to terrain
	1015	152	38	20.176	121	6.982	664627	4244804	Location of *in situ* count
A2000-0005	864	141	38	20.277	121	6.916	664719	4244992	
A4000-0001	1293	233	38	20.213	121	7.876	663323	4244846	
B1000-0001	774	260	38	20.606	121	7.711	663549	4245579	
B1000-0002	876	259	38	20.583	121	7.770	663464	4245533	
	876	259	38	20.577	121	7.770	663464	4245524	Location of second soil sample
B1000-0003	1072	261	38	20.585	121	7.891	663287	4245533	

B1000-0004	975	263	38	20.610	121	7.635	663368	4245581	
B3000-0001	893	235	38	20.376	121	7.694	663582	4245154	
B3000-0002	1037	245	38	20.421	121	7.619	663398	4245232	
B3000-0003	993	239	38	20.378	121	7.767	663476	4245154	
B3000-0004	1150	246	38	20.396	121	7.684	663305	4245185	
B5000-0001	787	246	38	20.529	121	7.754	663469	4245434	Location of SW corner of SAB
	720	246	38	20.537	121	7.711	663552	4245451	In-situ and soil sample at "Y"
C1000-0001	556	241	38	20.518	121	7.541	663799	4245421	
C1000-0002	475	233	38	20.510	121	7.477	663893	4245408	SAB SW corner for scan survey
	415	241	38	20.556	121	7.481	663885	4245493	C1-LMK-026 location
C1000-0003	411	221	38	20.497	121	7.412	663989	4245385	SAB SW corner for scan survey
	349	221	38	20.545	121	7.409	663991	4245475	C1-LMK025 location
C1000-0004	320	210	38	20.527	121	7.339	664093	4245443	SAB SW corner for scan survey
	289	213	38	20.543	121	7.334	664100	4245473	C1-LMK-024 location
	271	209	38	20.546	121	7.308	664138	4245479	C1-LMK-023a location
C1000-0005	281	187	38	20.515	121	7.268	664198	4245423	SAB SW corner for scan survey
	252	186	38	20.549	121	7.308	664218	4245485	C1-LMK-023 location
C1000-0006	310	166	38	20.502	121	7.202	664294	4245400	SAB SW corner for scan survey
	268	145	38	20.554	121	7.308	664333	4245493	*In situ* location
C1000-0007	340	158	38	20.493	121	7.170	664341	4245364	SAB SW corner for scan survey
	296	146	38	20.556	121	7.308	664395	4245498	C1-LMK-027 location
C3000-0001	474	214	38	20.447	121	7.410	664019	4245264	
C3000-0002	570	212	38	20.390	121	7.430	663966	4245187	
C3000-0003	467	174	38	20.402	121	7.217	664282	4245256	

	477	172	38	20.427	121	7.211	664284	4245262	
D1000-0001	534	349	38	21.003	121	7.309	664120	4246325	
	558	349	38	21.013	121	7.311	664116	4246342	
D1000-0002	556	17	38	21.008	121	7.149	664352	4246337	
D1000-0003	677	55	38	20.923	121	6.912	664701	4246189	
D1000-0004	539	34	38	20.956	121	7.063	664479	4246244	
D3000-0001	497	332	38	20.951	121	7.390	664003	4246225	
D3000-0002	416	340	38	20.924	121	7.332	664089	4246177	
D3000-0003	436	356	38	20.949	121	7.265	664185	4246225	
D3000-0004	397	11	38	20.922	121	7.201	664280	4246177	
E2000-0001	504	304	38	20.857	121	7.500	663846	4246048	
E2000-0002	532	267	38	20.668	121	7.570	663751	4245697	
E2000-0003	540	263	38	20.646	121	7.573	663749	4245656	
E2000-0004	455	276	38	20.712	121	7.522	663820	4245780	
F1000-0001	919	292	38	20.892	121	7.766	663458	4246105	
F1000-0002	853	306	38	20.990	121	7.666	663600	4246289	
F1000-0003	608	322	38	20.977	121	7.473	663882	4246271	
F1000-0004	1110	293	38	20.944	121	7.870	663304	4246198	
F1000-0005	1013	279	38	20.783	121	7.855	663332	4245900	SW corner of scan survey. Moved due to terrain
	976	279	38	20.782	121	7.830	663369	4245901	Location of *in situ* count
F1000-0006	1027	268	38	20.662	121	7.871	663314	4245676	SW corner of scan survey. Moved due to terrain
	990	268	38	20.662	121	7.845	663351	4245677	Location of *in situ* count
F1000-0007	864	265	38	20.639	121	7.771	663461	4245636	

G2000-0001	692	96	38	20.642	121	6.628	664833	4245671	
G2000-0002	680	113	38	20.525	121	6.865	664784	4245454	
G2000-0003	694	131	38	20.410	121	6.926	664699	4245239	
G2000-0004	430	83	38	20.715	121	6.987	664599	4245801	
H4000-0001	701	71	38	20.820	121	6.843	664805	4246000	
H4000-0002	326	34	38	20.849	121	7.135	664379	4246045	SW corner of scan survey. Moved due to terrain
	328	34	38	20.844	121	7.139	664373	4246035	Location of *in situ* count
H4000-0003	313	24	38	20.858	121	7.170	664328	4246061	SW corner of scan survey. Moved due to terrain
	313	24	38	20.870	121	7.171	664325	4246082	Location of *in situ* count
H4000-0004	588	63	38	20.848	121	6.929	664679	4246049	
I1000-0001	540	132	38	20.465	121	7.003	664586	4245339	Inside PV Array
I1000-0002	442	145	38	20.466	121	7.091	664457	4245337	Inside PV Array
J1000-0001	NA	NA	NA	NA	NA	NA	NA	NA	Road Survey
J1000-0002	NA	NA	NA	NA	NA	NA	NA	NA	Road Survey
Z9999-0001	0	0	38	20.665	121	7.247	664222	4245737	Center of Reactor Building

Appendix B

Detector Quality Control

1. In situ Quality Control

Quality control (QC) counts were performed several times per day during the execution of the *in situ* measurements. The QC routine consisted of a MCA gain check and adjustment (if necessary) and integration of peak counts in a common region of interest (ROI) to ensure consistent equipment performance. The gain check investigates positioning of the 1332 keV ^{60}Co photopeak in reference to MCA channel 227. An administrative limit of 10 channels per hour of gain shift was placed on the operation of the *in situ* system. After alignment, a secondary ^{60}Co standard was placed in a reproducible jig on the side of the SRA tripod and counted for 2 minutes. The QC spectra were logged to a field computer and ^{60}Co peak counts plotted for comparison with control limits of ±20%.

The region of interest (ROI) over which the QC spectra were integrated was from channel 214 to channel 242. This range was established to allow for approximately 50 keV below and above the ^{60}Co energy region. The control chart for *in situ* QC measurements is shown in Figure 1-1B.

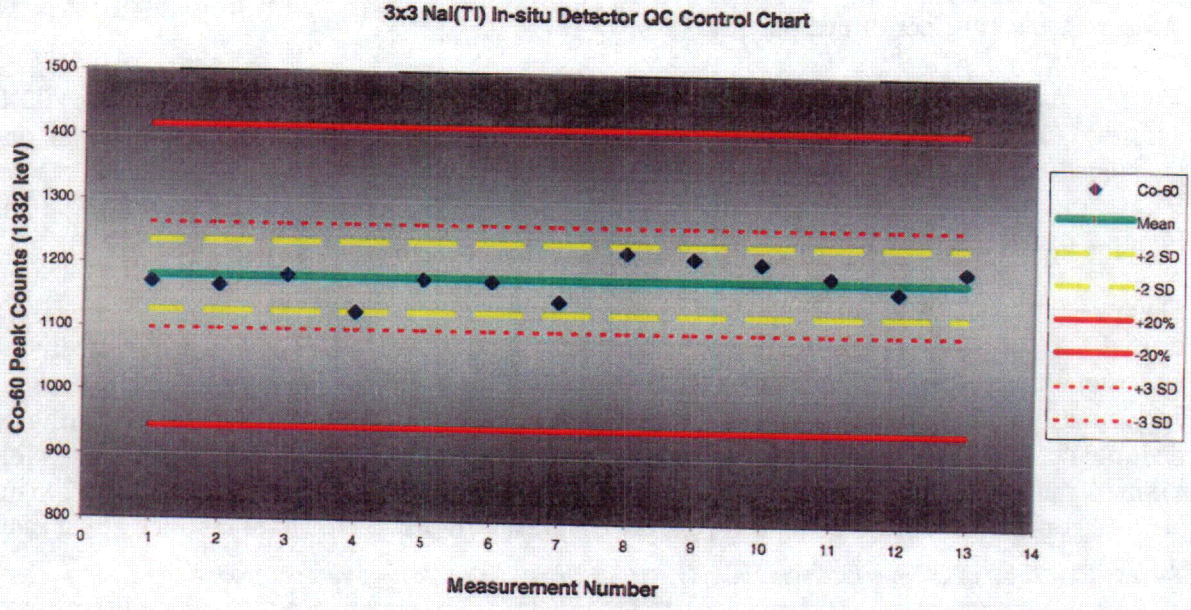

Figure 1-1B - Control Chart for in situ QC Measurements

C06

2. SMCM Quality Control

SMCM quality control (QC) measurements were performed prior to and after the successful completion of each SAB scan survey. This routine was designed such that each SAB was bound by a QC measurement. The QC routine consisted of a MCA gain check and adjustment (if necessary) and integration of peak counts in a common region of interest (ROI) from check sources to ensure consistent equipment performance. ^{60}Co and ^{137}Cs sources were alternately used throughout the survey for QC purposes. After alignment, sources were placed in identical fixtures on the sides of each 5x2 NaI(Tl) enclosure. The QC spectra were logged in the same fashion as normal survey data, using the SMCM software to log survey strips of data to the field computer with unique QC filenames.

However, near the midpoint of the survey the field team decided to reduce the number of QC measurements in half, from 1 per SAB to 1 per every 2 SABs. QC measurements were still performed at the beginning and end of each survey day. This decision did not impact the performance of the SMCM as increased survey throughput still allowed an average of 4 QC measurements to be performed per day.

The regions of interest (ROI) over which the QC spectra were integrated were: channels 202 to 245 for ^{60}Co, and channel 110 to 135 for ^{137}Cs. These ranges were established by maximizing the signal-to-noise ratio for each nuclide. Control charts were then generated for each detector for each nuclide. These Control Charts are shown in Figure 2-1B, Figure 2-2B, Figure 2-3B and Figure 2-4B.

There were 17 QC measurements that fell outside of 2 standard deviations (out of 218 total). Of these 17, 8 are believed to have occurred due to a slight detector gain shift due to temperature variation. Measurement data for these 8 are shown in Table 2-1B. It is believed that a systematic error contributed to these measurements since all share a common thread of failures occurring on multiple detectors at the same time. In particular, ^{60}Co QC measurements were more susceptible to small gain shifts due to smaller signal-to-noise ratios for the ^{60}Co check sources used. This is because contributions from natural ^{40}K can have a greater impact on the total reported count rate.

Table 2-1B – Table of QC measurements outside of 2 SD criteria. Data is in counts per second (cps)

QC #	Nuclide	Date	Time	Det 1	Det 2	Det 3	Det 4	Notes
13	Co-60	12/6/00	12:15	24.4	24.0	24.3	20.9	All detectors above 2 sd.
26	Co-60	12/12/00	11:54	20.0	18.0	19.4	15.8	All detectors below 2 sd.

The remaining 9 found to be outside of two standard deviations were found spread throughout the data set. The frequency of the remaining events falls within that expected at a 95% confidence level (9/218 = 4.1%). Thus, no further investigation was deemed necessary.

Co-60

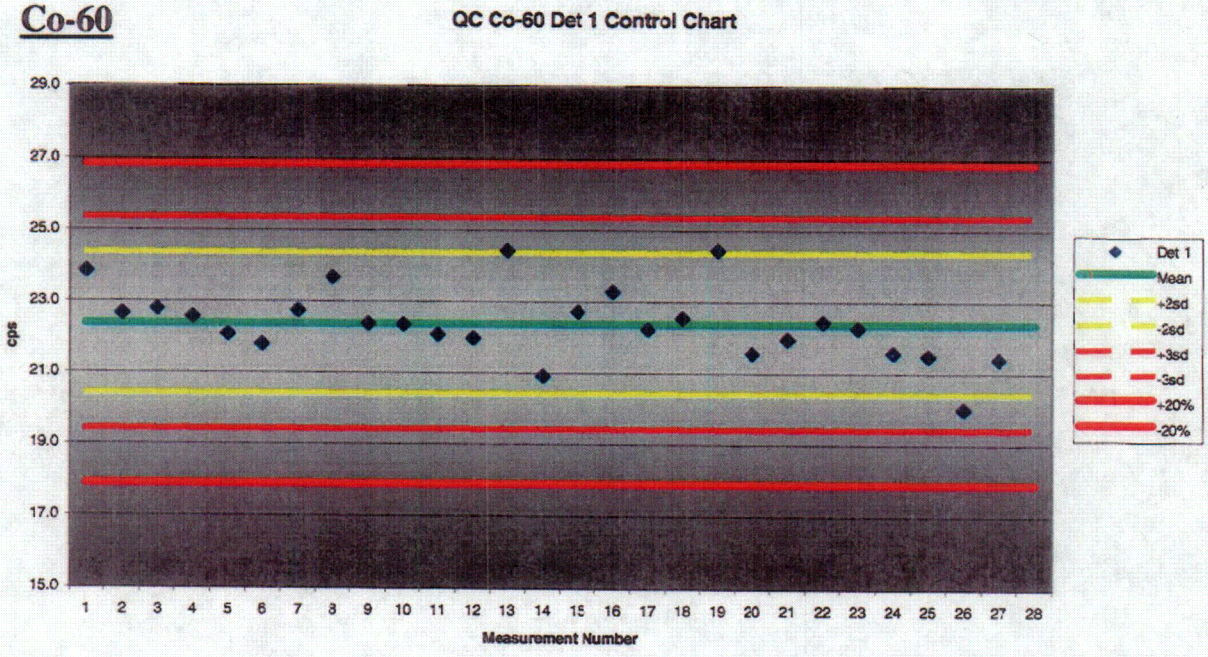

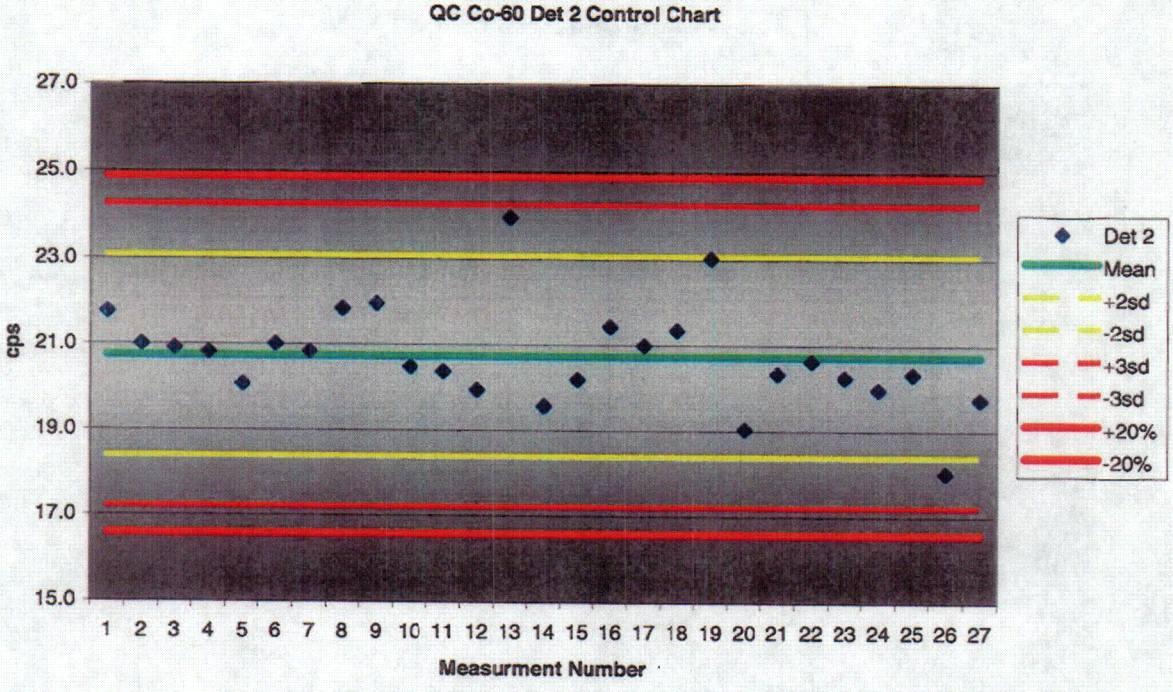

Figure 2-1B - Co-60 QC control charts for SMCM detectors 1 and 2.

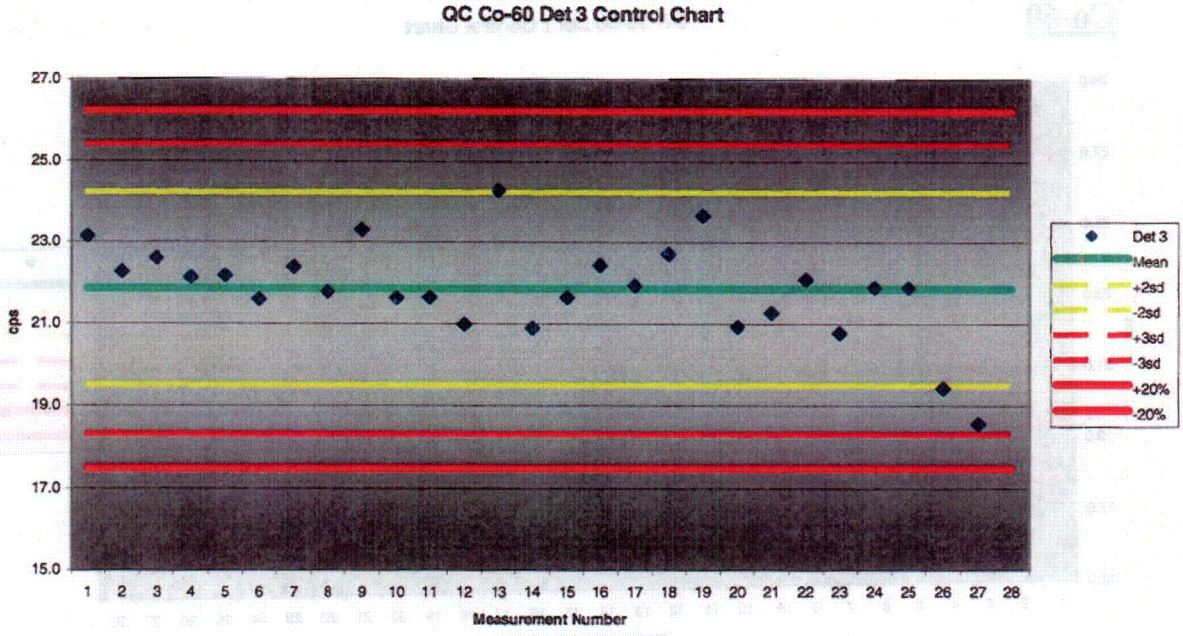

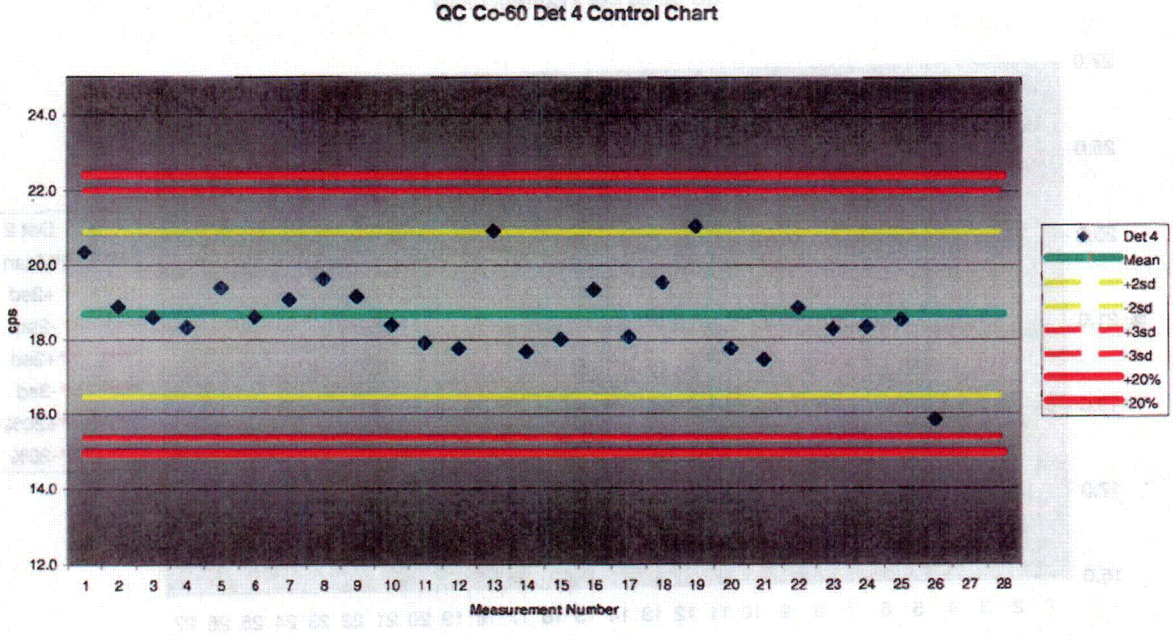

Figure 2-2B- Co-60 QC control charts for SMCM detectors 3 and 4.

Cs-137

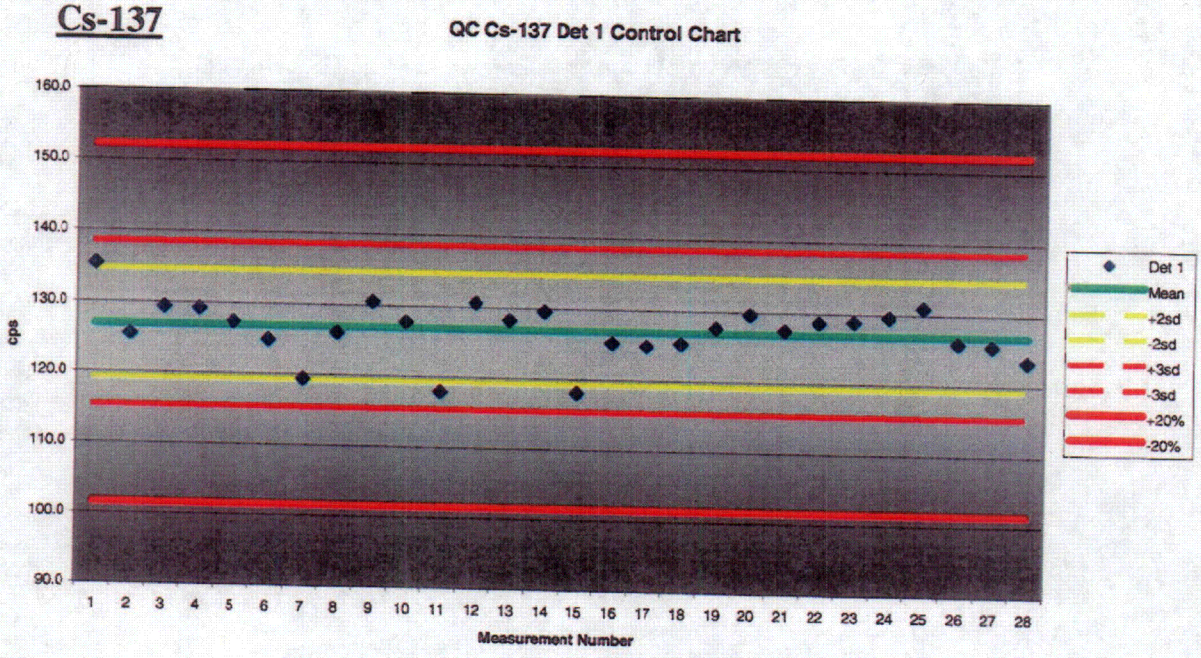

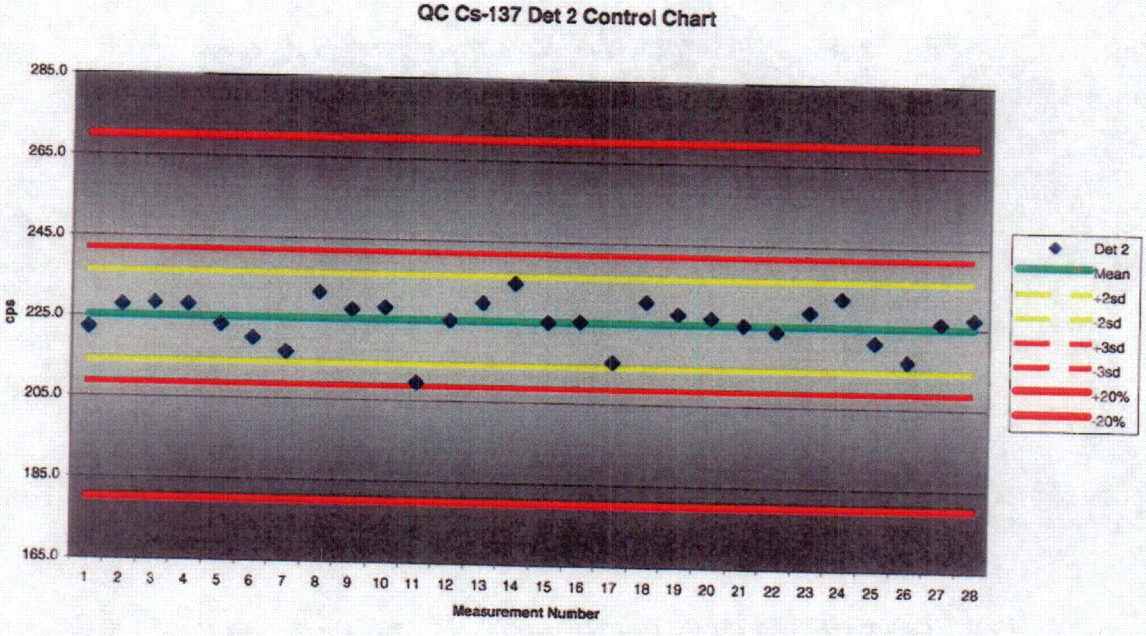

Figure 2-3B – Cs-137 QC control charts for SMCM detectors 1 and 2.

C09

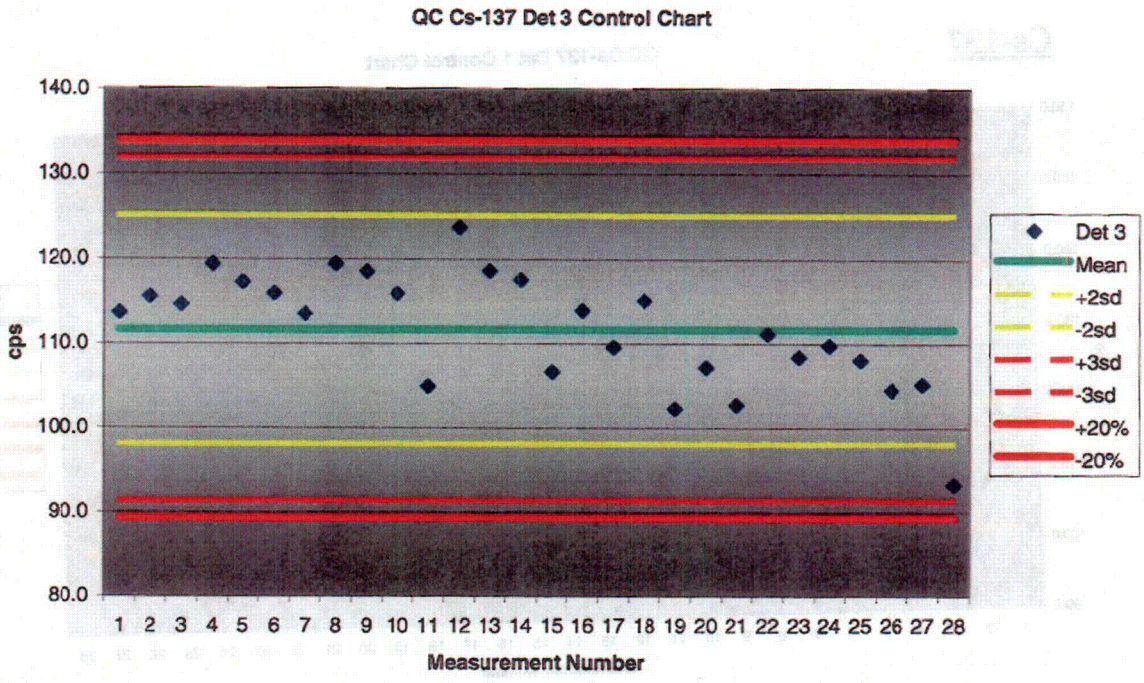

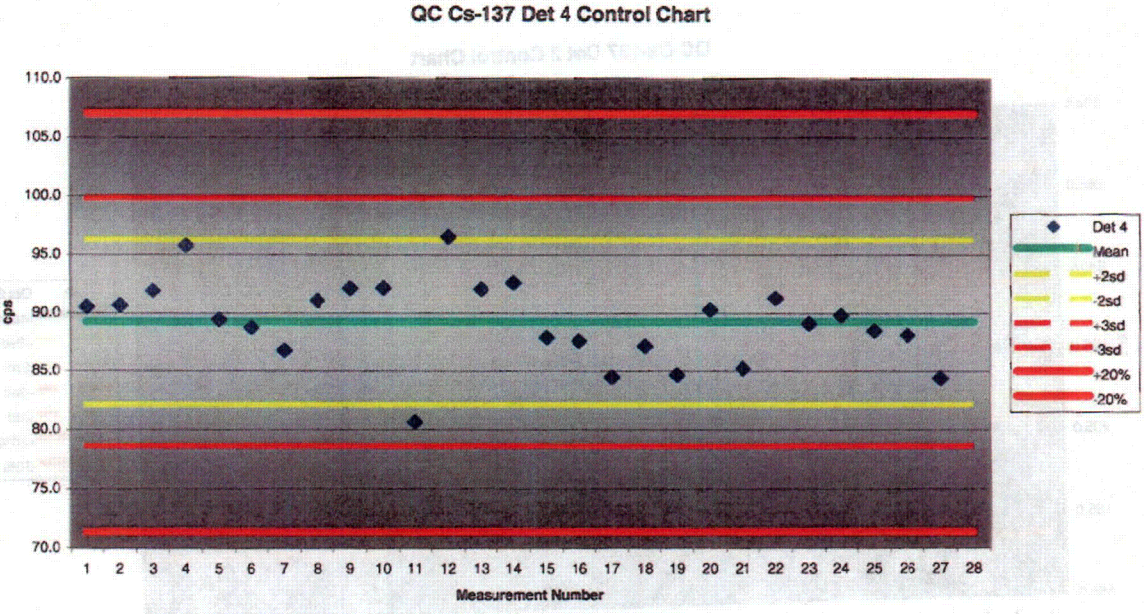

Figure 2-4B - Cs-137 QC control charts for SMCM detectors 3 and 4.

Appendix C

SRA Technical Note 01-001

Determination of Stripping Coefficients

SRA Tech Note no. 01-001 Rev. 1 Dated 06/26/01
Author: R.E. Burmeister

The SRA Subsurface Multi-spectral Contamination Monitor (SMCM) made use of the potassium (^{40}K) window in its data analysis. It was recognized that there would be spectral interferences from other primordial nuclides. This technical note describes the method used to account for the interferences and details the determination of certain parameters used in the calculations.

Spectral interferences among K, U and Th radiation occur due to the combined effects of full-energy-peak overlaps and gamma ray scattering in the source, in the transport path from source to detector, and as a result of partial absorption processes in the detector. There are standard methods to treat these interferences, and the traditional IAEA recommended method was applied. In this method, only the relative contributions from the Th source into the U and K windows, denoted as α and β, respectively, and the uranium series contribution to K, denoted as γ, were taken into account (IAEA 1979). The contributions are displayed symbolically in the following equations.

$$Th_c = Th - Th_b$$
$$U_c = U - U_b - \alpha Th_c$$
$$K_c = K - K_b - \beta Th_c - \gamma U_c$$

where

K_b, U_b, Th_b are background count rates,
K, U, Th are uncorrected count rates, and
K_c, U_c, Th_c are corrected count rates.

The stripping coefficients or stripping ratios are defined as the ratio of the number of counts due to a nuclide in other windows to the number of counts in the window for the nuclide. The ratios are usually determined from calibration pads which are large concrete pads that are doped with uranium, thorium, and potassium sources.

Stripping ratios for a few cylindrical detectors are available. The 5x2 detectors used by the SMCM were not part of the available lists. It was therefore necessary to estimate the ratios for the 5x2s from the lists of ratios for other detectors. For each of the detectors in the list in Table 1-1C, the source-detector geometry was the same, and the detectors were all cylinders. The quantity that changed among the detectors was the volume, or equivalently the mass, since the detectors had the same density. For a given photon energy, the mass-attenuation coefficient is the same for the detectors, but the varying volumes imply varying amounts of event collection. Thus, the stripping coefficients should be functions of the photon interaction collection volume of the detectors.

The data for the stripping coefficients for the standard detector sizes in Table 1-1C were plotted against detector volume. The plot is shown in Figure 1-1C. The values for α, β, γ were read off of the plot for the volume of the 5x2 detectors for a detector volume of 2574 cc.

The values are given in Table 1-1C in bold.

Table 1-1C. Stripping Coefficients for some Standard Detectors (Grasty1997) and the fitted SRA 5x2 (in bold).

Detector	α	β	γ
3x3	0.71	0.88	1.0
5x5	0.43	0.62	0.95
9x4	0.39	0.52	0.90
5x2	**0.63**	**0.81**	**0.99**

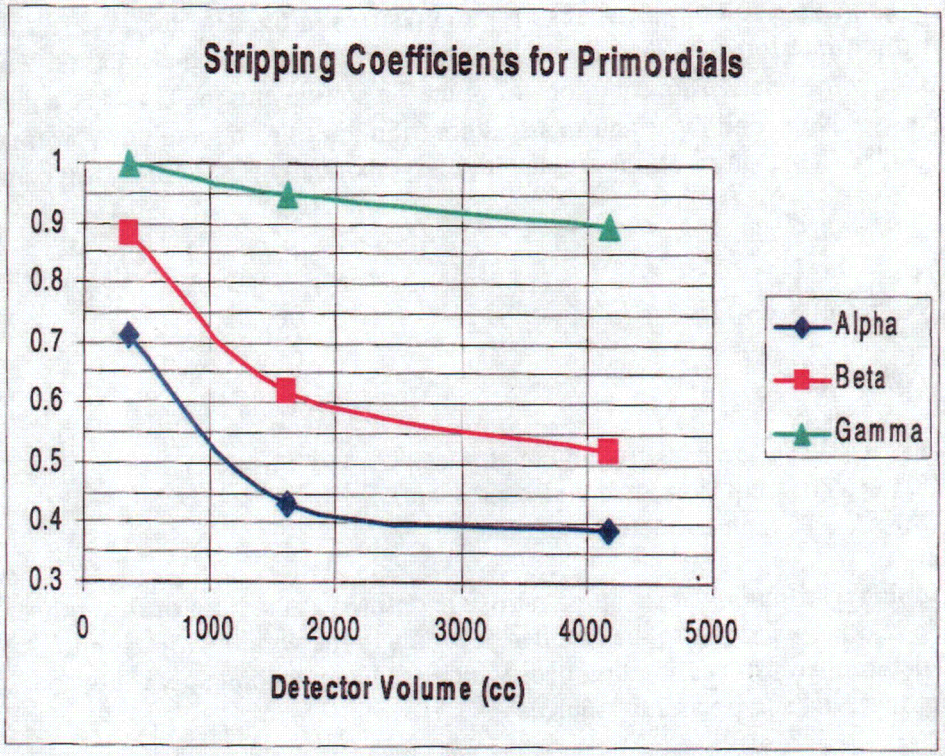

Figure 1-1C. Plot of Stripping Coefficients in Table 1 with smooth line interpolation

(Grasty 1997) Grasty, Bob. *Standardization of Airborne Gamma-Ray Surveys.* Presentation at HPS 42nd Annual Meeting, Summer 1997.

(IAEA 1979) International Atomic Energy Agency. *Gamma Ray Surveys in Uranium Exploration.* Technical Report Series 186. International Atomic Energy Agency, Vienna.

Appendix D

SRA Technical Note 01-004

Determination of the "Gator Factor"

SRA Tech Note no. 01-004 Dated 01/08/01
Author: R.E. Burmeister

When the SRA Subsurface Multi-spectral Contamination Monitor (SMCM) is deployed with multiple detectors on a survey platform, the possibility exists that the platform will obstruct the field of view of some of the detectors. This obstruction of the field of view results in different responses from the detectors. When surveying a field area for background, the detectors should have as similar a response as possible. This technical note describes the determination of shielding factors that account for the obstructed field of view and put the detectors on the same response basis.

The method begins with the collection of a series of region-of-interest (ROI) integrations. In general, there are more than one region-of-interest. Each detector collects spectral data that can be integrated to determine ROI values. One of the detectors with an unobstructed view is then chosen to be the basis for comparing the responses of the detectors. The ratio of ROIs of the other detectors to the chosen detector, one ratio per ROI, are numbers that report how similarly the other detectors responded compared to the basis detector, and are also numbers that can be used to scale the responses of the other detectors so that shielding effects from obstructed views are removed.

The ratios are determined for a number of background surveys until the statistics yield a standard deviation of 1-2% for each ROI, and then the mean ratio for each ROI-detector combination is recorded. If the standard deviation of the mean ratios for all ROIs for a particular detector is also 1-2%, then the mean of the mean ratios per detector is used.

For example, assume four detectors and three regions-of-interest and five initial surveys. Also assume that detector 1 was chosen as the basis detector. Thus, the calculation of the ratio of detectors 2, 3, and 4 to detector 1 for each ROI would yield a table of ratios like that below, filled with hypothetical data.

Table 1-1D. Hypothetical Table of Ratios for Three Regions-of-Interest and Four Detectors

	ROI 1			ROI 2			ROI 3		
survey	2	3	4	2	3	4	2	3	4
1	0.961	0.953	1.031	0.982	0.966	1.007	0.978	0.935	1.074
2	0.950	0.936	1.024	0.948	0.971	1.013	0.968	0.948	1.048
3	0.955	0.950	1.048	0.952	0.973	1.027	1.004	0.968	1.072
4	0.978	0.945	1.046	0.925	1.038	1.020	1.007	0.934	1.059
5	0.967	0.956	1.025	0.916	0.919	0.974	1.026	1.000	1.088
Mean	0.962	0.948	1.035	0.944	0.973	1.008	0.997	0.957	1.068

The mean reported in Table 1-1D is the mean of the corresponding five ratios; this is the mean ratio for each ROI-detector combination. At this point, if a particular detector's mean ratios are averaged for all ROIs, the result would be the mean of the mean ratios referred to above. For ROI 1, the above means, imply that for the five surveys, detector 2 was on average 96% of detector 1. Similarly, detectors 3 and 4 were 95% and 104% of detector 1. There are similar numbers for the other regions-of-interest. To place the detectors on the same basis as detector 1, future responses would need to be divided by these ratios.

Appendix E

SRA Technical Note 01-006

In situ Calibration Factor Methodology

1. Objective

This document develops calibration factors for the three inch by three inch sodium iodide (3-by-3 NaI) detector system employed at the Rancho Seco site for *in situ* counting of designated areas from December 3 through December 13, 2000. Factors are developed for the common power plant nuclides ^{60}Co, ^{134}Cs, and ^{137}Cs for deposition geometries and for uniform distribution in soil. Factors are also provided for selected primordial nuclides for uniform distributions. The fission/activation product nuclides were included in the uniform distribution factors to provide values to use for establishing detection limits in cases where the use of deposition factors would be inappropriate.

2. Summary

SRA's *in situ* system consisted of a NaI(Tl) detector and electronics enclosed in a nominal free-in-air tripod geometry at a fixed height of 1 meter above the ground. The detector was a Bicron model 3M3/3, serial number AA-4631-I , coupled to an EG&G ORTEC model 296 ScintiPak solid-state tube base, serial number 707. The Scintipack is equipped with integral high voltage power supplies and preamplifier stage in each unit. An ORTEC MicroNOMAD portable MCA, serial number 355, provided the amplifier stage and the analog-to-digital conversion.

The calibration factors developed in this document for aged deposition are given in Table 2-1E below. Factors for other deposition geometries (fresh deposition and an infinite plane) may be found in section 5.1. Table 2-2E gives the factors for uniform distributions. All of the factors are for uncollimated 3-by-3 NaI detectors at a height of one meter above the ground (measured to the detector's face). The calibration factors for the uniformly-distributed power plant nuclides inherently assume that the source is well mixed in the soil. These factors should not be applied to characterize sources where this is not the case. (One would not normally encounter cases where man-made nuclides could be modeled as a uniform distribution in soil).

Table 2-1E Calibration factors for in situ counting of aged deposition ($\alpha/\rho = 0.0625$) at a height of one meter above the soil

Nuclide	Energy (MeV)	Intensity (γs^{-1} per Bq)	N_0/ϕ (cpm per γ cm^{-2} s^{-1})	N_f/N_0	ϕ per unit source flux in soil	Calibration Factor cpm per Bq per m^2)	Calibration Factor (cpm per µCi per m^2)
^{134}Cs	0.56932	0.1543	1.26E+03	1	0.2600	5.06E-03	1.87E+02
^{134}Cs	0.6047	0.976	1.23E+03	1	0.2700	3.25E-02	1.20E+03
^{134}Cs	0.79585	0.854	1.09E+03	1	0.3000	2.80E-02	1.04E+03
^{137}Cs	0.66165	0.8512	1.19E+03	1	0.2788	2.81E-02	1.04E+03
^{58}Co	0.81076	0.994	1.08E+03	1	0.3000	3.23E-02	1.19E+03
^{60}Co	1.17322	1	8.44E+02	1	0.3437	2.90E-02	1.07E+03
^{60}Co	1.33249	1	6.77E+02	1	0.3617	2.45E-02	9.06E+02

Table 2-2E Calibration factors for in situ counting of uniformly-distributed sources ($\alpha/\rho = 0$) at a height of one meter

Nuclide	Energy	Intensity (γs^{-1} per Bq)	N_0/ϕ (cpm per g cm^{-2} s^{-1})	N_f/N_0	ϕ (g cm^{-2})	Calibration Factor (cpm per Bq per gram)	Calibration Factor (cpm per µCi per gram)
^{134}Cs	0.569	0.1543	1.26E+03	1	5.7	1.11E+03	4.10E+07
^{208}Tl	0.583	0.842	1.25E+03	1	5.8	6.11E+03	2.26E+08
^{134}Cs	0.605	0.976	1.23E+03	1	5.9	7.11E+03	2.63E+08
^{214}Bi	0.609	0.463	1.23E+03	1	5.9	3.36E+03	1.24E+08
^{137}Cs	0.662	0.8512	1.19E+03	1	6.1456	6.20E+03	2.30E+08
^{134}Cs	0.796	0.854	1.09E+03	1	6.7	6.26E+03	2.32E+08
^{58}Co	0.811	0.994	1.08E+03	1	6.8	7.32E+03	2.71E+08
^{214}Bi	1.12	0.151	8.55E+02	1	8	1.03E+03	3.82E+07
^{60}Co	1.173	1	8.44E+02	1	8.1472	6.87E+03	2.54E+08
^{60}Co	1.332	1	6.77E+02	1	8.7504	5.92E+03	2.19E+08

3. Technical Approach

The parameter of interest in *in situ* gamma ray spectrometry is the ratio between the count rate in the full-energy peak of interest and the corresponding quantity of the nuclide of interest in the soil below (either per unit mass or per unit area). This parameter is known as the calibration factor. The general expression employed in establishing calibration factors for *in situ* gamma ray spectrometry is

$$\frac{N_f}{A} = \left(\frac{N_f}{N_o}\right)\left(\frac{N_o}{\phi}\right)\left(\frac{\phi}{A}\right) \qquad (3\text{-}1E)$$

where each ratio in the above expression is defined as follows (Helfer and Miller 1988).

$\frac{N_f}{A}$ is the calibration factor desired. The dimensions are count rate (cpm, typically) per unit inventory (Bq m^{-2}) or per unit concentration (Bq g^{-1}) of the nuclide of interest in the soil.

$\frac{N_f}{N_o}$ is the angular correction factor for the detector at the energy of interest and for a given source distribution.

$\frac{N_o}{\phi}$ is the detector peak response, which is the peak count rate per unit uncollided flux from a plane-parallel source of the photon energy of interest.

$\frac{\phi}{A}$ is the total uncollided flux (for the photon energy of interest) arriving at the detector per unit inventory or concentration in the soil.

To establish a calibration factor for a nuclide of interest, the three ratios in Equation 3-1E are determined for a given detector configuration and source distribution. Note that the calculated calibration factor is not strongly influenced by the estimate of the source distribution, so inaccuracies in this estimation should not adversely affect the calculated factor. This is due to the fact the ratio between the uncollided flux at the detector and the source inventory or concentration does not vary significantly with source distribution (EML 1990).

The sections that follow describe the three factors from Equation 3-1E and how these are established. Values are given for each factor for the 3-by-3 NaI detectors. These factors are then used to calculate calibration factors for the detectors for three different deposition geometries and for uniform distributions.

4. Description of Individual Factors

4.1 Angular Correction Factor (N_θ/N_0)

The angular correction factor N_θ/N_0 depends on both the detector and the source geometry. It corrects for the fact the cylindrical detector does not respond isotropically to sources incident from different angles with respect to its vertical axis (when oriented normal to the ground). Values of N_θ/N_0 for intrinsic germanium (Ge) detectors have been published by Helfer and Miller (1988) as a function of energy and detector length-to-diameter ratio (L/D) for planar and uniform sources. ("Uniform" means constant source concentration with depth, and refers to the distribution of the primordial species within the soil. "Planar" means a surface source with uniform dispersion, i.e., an infinite plane source.) However, no such data were identified for NaI detectors. Hence, for the purpose of this document, the angular correction factor for the 3-by-3 NaI detector was assumed to be unity. This assumption is supported by the data given by Helfer and Miller that show, for an intrinsic Ge detector with a length-to-diameter ratio (L/D) of unity, the angular correction factor deviates from unity by no more than 4% for energies up to 2.5 MeV for either the uniform or planar source geometries. The assumption of unity for the angular correction factor for the 3-by-3 detector also makes sense intuitively, as one would not expect any significant difference in response with zenith angle for a symmetric detector geometry.

4.2 Peak Count Rate per Unit Uncollided Flux (N_0/ϕ)

The values of N_0/ϕ for a given detector can be obtained by counting point sources of the nuclides of interest at a distance of at least one meter from the face of the detector (Helfer and Miller 1988). At this distance, a point source provides a good approximation of a plane-parallel field. N_0/ϕ is computed by dividing the observed peak count rate by the flux at the detector. The flux is computed by dividing the source photon emission rate by $4\pi r^2$ and correcting (if necessary) for attenuation by air and the source holder. The distance r to be used depends on the photon energy. For energies > 1 MeV, r should be taken as the distance to the center of the crystal; and for energies < 100 keV, the distance should be to the detector face (EML 1990). For energies in between these values, the distance to be used can be computed using the mean free path in sodium iodide for the photon energy of interest. However, one should be careful when doing so to be sure that the mean free path is not greater than the location of the midpoint of the crystal. If this does occur, then r should be chosen to correspond with the detector midpoint. The preferred dimensions of N_0/ϕ are cpm per photon cm^{-2} $second^{-1}$.

Values of N_0/ϕ were established for each of the detector system by making measurements at a distance of one meter using NIST traceable ^{137}Cs and point sources, serial numbers 619-38-1 and 578-32-17, respectively.. The original activities were 9.301 μCi for the ^{137}Cs standard (on 7/1/98) and 0.8029 μCi for the ^{60}Co standard (on 7/1/98). For the ^{60}Co measurements, an additional secondary standard ^{60}Co source was also used to increase the total photon flux at the detector face. The secondary standard was calibrated using the primary standard 578-32-17. The total ^{60}Co activity used was 0.963 μCi. The calibration certificates for these standards are included in Appendix J. Each source was counted for a period of 5 minutes, preceded by a 10 minute background count. Net count rates for each photo-peak were established by subtracting the

background counts from the gross counts for each energy region. These data are given in Table 4-1E below.

Table 4-1E Calibration data for SRA in situ System

Nuclide	Energy (keV)	Gross Count Rate (cps)	Background Count Rate (cps)	Net Count Rate (cps)	Uncertainty (2σ)
^{137}Cs	662	44.87	4.46	40.41	0.81
^{60}Co	1173	7.22	3.52	3.70	0.38
^{60}Co	1332	4.90	1.93	2.97	0.30

Figure 4-1E shows the calculation of the N_0/ϕ values using the measured net count rates from the tables above.

Assay activity (μCi) for the ^{137}Cs source = 9.301
Assay date for the ^{137}Cs source = 7/1/98
Assay activity (μCi) for the ^{60}Co source = 0.963
Assay date for the ^{60}Co source = 12/22/00
^{137}Cs half-life (days) = 11019.59
^{60}Co half-life (days) = 1925.23
Cs-137 Measurements date = 12/13/00
Co-60 Measurements date = 12/22/00

Cs-137 Activity (μCi) on measurements date = 8.791
Co-60 activity (μCi) on measurements date = 0.963

Nuclide	Photon Energy (keV)	Photon Intensity	Net Peak Area (cpm)	cpm/μCi	r (cm)	N_0/ϕ
Cs-137	661.65	0.85	2.42E+03	2.76E+02	103.81	1.19E+03
Co-60	1173.22	1.00	2.22E+02	2.31E+02	103.81	8.44E+02
Co-60	1332.49	1.00	1.78E+02	1.85E+02	103.81	6.77E+02

Figure 4-1E Calculation of N_0/ϕ values for SRA in situ system.

The N_0/ϕ value for the common plant mix nuclide ^{134}Cs was established by linear interpolation of the data for ^{137}Cs and ^{60}Co peaks. These values, along with the values measured using the traceable sources, are summarized in Table 4-2E and Figure 4-2E below.

Table 4-2E N_0/ϕ values for SRA In situ System. Shaded cells represent interpolated/extrapolated data points.

Nuclide	Energy	N_0/ϕ (cpm per γ cm^{-2} s^{-1})
^{134}Cs	0.569	1.26E+03
^{134}Cs	0.605	1.23E+03
^{137}Cs	0.662	1.19E+03
^{134}Cs	0.796	1.09E+03
^{60}Co	1.173	8.44E+02
^{60}Co	1.332	6.77E+02
^{40}K*	1.461	6.04E+02

*^{40}K is applied to uniformly distributed case only.

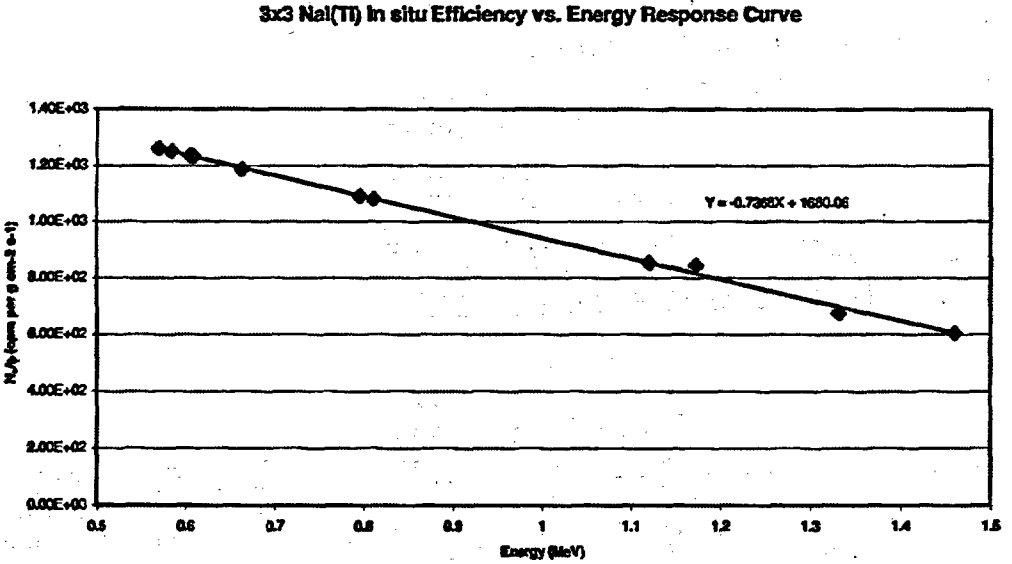

Figure4-2E 3x3 NaI(Tl) In situ Efficiency vs. Energy Response Curve

4.3 Total Uncollided Flux per Unit Source Inventory or Concentration (ϕ/A)

The factor ϕ/A is not detector dependent, but is a function of soil composition and density, air attenuation and the distribution of the source in the soil. Values of ϕ for sources in soil having strengths of either 1 photon $gram^{-1}$ $second^{-1}$ (for a uniform source) or 1 photon cm^{-2} $second^{-1}$ (for sources exponentially distributed with depth or for planar sources), are given by Helfer and Miller (1988). These data are reproduced as Table 4-3E. Note these data are flux (at the detector) per unit photon emission in soil. Hence, the data have dimensions of g cm^{-2} for the uniform source and are

dimensionless for the distributed (deposited) sources. To get the quantity desired (ϕ/A), these values must be multiplied by the intensity for the photon of interest. Doing so gives ϕ/A in terms of g cm^{-2} per Bq per $\gamma\ s^{-1}$ for the uniform source and $\gamma\ s^{-1}\ Bq^{-1}$ for the distributed sources.

The parameter α/ρ is a measure of the source depth profile, where the profile is assumed to be exponential. α is the inverse of the relaxation length and ρ is the soil density. Thus, α/ρ equals zero for the uniform (primordial) source geometry (where the source profile is a constant) and equals infinity for an infinite plane. Deeply distributed sources have values of α/ρ that are less than 0.1, where a range $0.1 \leq \alpha/\rho \leq 0.5$ would be characteristic of fallout from historical weapons testing that has not penetrated far into the soil (Helfer and Miller 1988). In the case of aged fallout in the U.S., Helfer and Miller give ranges for α/ρ of 0.03 to 0.2 for open fields in areas having moist climates and 0.2 to 1.0 for semi-arid regions. The α/ρ value of 6.25 in Table 2-1E corresponds to fresh deposition with little penetration into the soil.

It should be noted that while the parameter α/ρ is favored domestically for characterizing source profiles in soil, the ICRU uses a different parameter for the same purpose (ICRU 1994). They chose to define a parameter that is essentially the inverse of α/ρ called the relaxation mass per unit area, β. β has the dimensions of g cm^{-2}. The most notable difference between β and α/ρ is that β is defined in such a manner that the soil density profile can be accounted for, whereas α/ρ can only be defined for constant soil density. Beyond this, the only important thing to remember is that β is the inverse of α/ρ, and so $\beta = 0$ corresponds to the infinite plane (where $\alpha/\rho = \infty$) and $\beta = \infty$ corresponds to the uniform source (where $\alpha/\rho = 0$).

Table 4-3E ϕ values per unit source strength* as a function of energy and source distribution published by Helfer and Miller (1988)

Source energy (keV)	(α/ρ) 0 (Uniform)	0.0625	0.206	0.312	0.625	6.25	∞ (plane)
50	1.4403	0.0816	0.2245	0.3049	0.4748	1.147	1.577
100	2.7744	0.1458	0.3627	0.4708	0.6786	1.359	1.710
150	3.3264	0.1702	0.4103	0.5261	0.7438	1.427	1.775
200	3.9056	0.1843	0.4550	0.5770	0.8018	1.483	1.804
250	4.0640	0.2008	0.4697	0.5910	0.8185	1.506	1.863
364	4.7184	0.2268	0.5158	0.6429	0.8775	1.578	1.933
500	5.3904	0.2519	0.5595	0.6918	0.9334	1.650	1.995
662	6.1456	0.2788	0.6041	0.7412	0.9889	1.719	2.054
750	6.5312	0.2919	0.6257	0.7649	1.015	1.752	2.084
1000	7.5280	0.3245	0.6769	0.8209	1.077	1.830	2.151
1173	8.1472	0.3437	0.7067	0.8531	1.113	1.874	2.189
1250	8.4384	0.3523	0.7198	0.8675	1.129	1.895	2.205
1333	8.7504	0.3617	0.7336	0.8826	1.145	1.914	2.224
1460	9.1472	0.3731	0.7511	0.9011	1.166	1.941	2.247
1765	10.091	0.3997	0.7897	0.9428	1.211	1.997	2.294
2004	10.818	0.4188	0.8173	0.9725	1.243	2.036	2.334
2250	11.397	0.4357	0.8414	0.9982	1.271	2.071	2.358
2500	12.173	0.4536	0.8667	1.025	1.300	2.105	2.385

**For the uniform profile ($\alpha/\rho = 0$), the source strength is one gamma per second per gram for soil at all depths. For the exponential profiles (deposited nuclides), the source strength is one gamma per cm^2 per second. Thus, the data for the uniform source have dimensions of g cm^{-2} and those for the exponential sources are dimensionless.*

5. Results

5.1 Calibration Factors for Depositions of Common Power Plant Nuclides

Calibration factors for the NaI detector system for the common power plant nuclides ^{134}Cs, ^{137}Cs, and ^{60}Co have been estimated as follows. Values for the peak count rate per unit uncollided flux (also known as the response factor) for each system were established using the peak count rates measured using the NIST traceable ^{137}Cs and ^{60}Co sources. The calibration factor for ^{134}Cs was inferred from this data through linear interpolation. Values for the angular correction factors were assumed to be unity, as discussed in section 4.1. Values for the uncollided flux per unit source concentration or inventory were taken from Table 4-3E above. Using these values, calibration factors for *in situ* counting were established for three deposition geometries for the detector at a distance of one meter above the ground. The three source geometries were aged deposition (α/ρ = 0.0625), fresh deposition (α/ρ = 6.25) and an infinite plane ($\alpha/\rho = \infty$).

The ϕ values used in the calculation of the calibration factors for deposited nuclides for the detector system are given in Table 5-1E. These values were established from linear interpolation of the data in Table 4-3E where necessary.

Table 5-1E ϕ values used in the calculation of the calibration factors for deposited nuclides

		Uncollided Flux per Unit Source (ϕ) (dimensionless)		
Nuclide	Energy (MeV)	Aged	Fresh	∞-plane
^{134}Cs	0.56932	0.26	1.68	2.02
^{134}Cs	0.60470	0.27	1.69	2.03
^{134}Cs	0.79585	0.30	1.77	2.10
^{137}Cs	0.66165	0.2788	1.719	2.054
^{58}Co	0.81076	0.30	1.77	2.10
^{60}Co	1.17322	0.3437	1.874	2.189
^{60}Co	1.33249	0.3617	1.914	2.224

To compute the calibration factors for *in situ* soil counting for deposited nuclides, the values given in Table 4-2E and Table 5-1E were substituted into Equation 3-1E. The ϕ values from Table 5-1E are converted to ϕ/A by multiplying by the appropriate photon intensity. The calculated factors are then multiplied by 1×10^{-4} m^2 per cm^2 to get the desired dimensions. The factors are given in terms of both cpm per Bq per square meter (current convention) and cpm per μCi per square meter.

Table 5-2E Calibration factors for In situ *counting of aged deposition ($\sigma/\rho = 0.0625$) at a height of one meter above the soil*

Nuclide	Energy (MeV)	Intensity (γs^{-1} per Bq)	N_0/ϕ (cpm per $\gamma cm^{-2} s^{-1}$)	N_f/N_0	ϕ per unit source flux in soil	Calibration Factor cpm per Bq per m^2)	Calibration Factor (cpm per μCi per m^2)
^{134}Cs	0.56932	0.1543	1.26E+03	1	0.2600	5.06E-03	1.87E+02
^{134}Cs	0.6047	0.976	1.23E+03	1	0.2700	3.25E-02	1.20E+03
^{134}Cs	0.79585	0.854	1.09E+03	1	0.3000	2.80E-02	1.04E+03
^{137}Cs	0.66165	0.8512	1.19E+03	1	0.2788	2.81E-02	1.04E+03
^{58}Co	0.81076	0.994	1.08E+03	1	0.3000	3.23E-02	1.19E+03
^{60}Co	1.17322	1	8.44E+02	1	0.3437	2.90E-02	1.07E+03
^{60}Co	1.33249	1	6.77E+02	1	0.3617	2.45E-02	9.06E+02

Table 5-3E Calibration factors for in situ counting of an infinite plane ($\alpha/\rho = \infty$) at a height of one meter

Nuclide	Energy (MeV)	Intensity (γs^{-1} per Bq)	N_0/ϕ (cpm per γ cm^{-2} s^{-1})	N_ϕ/N_0	ϕ per unit source flux in soil	Calibration Factor (cpm per Bq per m^2)	Calibration Factor (cpm per µCi per m^2)
^{134}Cs	0.56932	0.1543	1.26E+03	1	2.0200	3.93E-02	1.45E+03
^{134}Cs	0.6047	0.976	1.23E+03	1	2.0300	2.45E-01	9.05E+03
^{134}Cs	0.79585	0.854	1.09E+03	1	2.1000	1.96E-01	7.26E+03
^{137}Cs	0.66165	0.8512	1.19E+03	1	2.0540	2.07E-01	7.67E+03
^{58}Co	0.81076	0.994	1.08E+03	1	2.1000	2.26E-01	8.36E+03
^{60}Co	1.17322	1	8.44E+02	1	2.1890	1.85E-01	6.83E+03
^{60}Co	1.33249	1	6.77E+02	1	2.2240	1.51E-01	5.57E+03

5.2 Calibration Factors for Uniform Distributions

Calibration factors were established for uniform distribution in soil following the same methodology as for the deposition factors established in the previous section. Factors were established for the common power plant nuclides ^{134}Cs, ^{137}Cs, and ^{60}Co; and for selected primordial nuclides. The factors given for the power plant nuclides should be applied with caution, as one would not typically encounter a distribution of these in soil that would represent a uniform distribution. They have been provided here as it is felt they would be applicable at the Rancho Seco site for characterizing any material inadvertently transferred within the property, assuming the material was well-mixed in the soil. Note the calibration factors for characterizing uniform distributions have different dimensions than those for depositions given in the previous section. The dimensions for the factors in this section are cpm per Bq (or µCi) per gram.

The N_0/ϕ values determined from the measurements with the traceable ^{137}Cs and ^{60}Co sources were used to establish N_0/ϕ values for selected gamma lines from the primordial nuclides. This was done by interpolating or extrapolating using the two energies nearest the energy of interest. Though it is a prominent line used to quantify natural thorium from *in situ* measurements, the 2.615 MeV photon from ^{208}Tl was not included. This was because it was deemed inappropriate to extrapolate from 1.3 MeV (upper ^{60}Co peak) to 2.6 MeV. The same was true for the 1.764 MeV ^{214}Bi line, and its predecessor, the 0.352 MeV line of ^{214}Pb (from the ^{238}U series). The N_0/ϕ values used to calculate the calibration factors for uniformly-distributed nuclides are given in Table 5-4E. The values for the power plant nuclides come from Table 4-3E.

Table 5-4E N_0/ϕ values used in the calculation of the calibration factors for nuclides uniformly distributed in soil

Nuclide	Energy	Intensity (γs^{-1} per Bq)	N_0/ϕ (cpm per γ $cm^{-2} s^{-1}$)
^{134}Cs*	0.569	0.1543	1.26E+03
^{208}Tl (Th series)*	0.583	0.842	1.25E+03
^{134}Cs	0.605	0.976	1.23E+03
^{214}Bi (U series)*	0.609	0.463	1.23E+03
^{137}Cs	0.662	0.8512	1.19E+03
^{134}Cs*	0.796	0.854	1.09E+03
^{58}Co	0.811	0.994	1.08E+03
^{214}Bi (U series)*	1.12	0.151	8.55E+02
^{60}Co	1.173	1	8.44E+02
^{60}Co	1.332	1	6.77E+02
^{40}K*	1.461	0.1067	6.04E+02

**Results based on linear interpolation/extrapolation of the results for the 662 keV Cs-137 peak and the 1173 keV Co-60 peak*

The ϕ values used in the calculation of the calibration factors are given in Table 5-3E. These values were established from linear interpolation of the data in Table 4-1Ewhere necessary.

Table 5-5E ϕ values used in the calculation of the calibration factors for uniform distribution ($\alpha/\rho = 0$)

Nuclide	Energy (MeV)	ϕ (g cm^{-2})
^{208}Tl (Th series)	0.583	5.8
^{40}K	1.461	9.1472
^{214}Bi (U series)	1.120	8.0
^{214}Bi (U series)	0.609	5.9
^{134}Cs	0.569	5.7
^{134}Cs	0.605	5.9
^{134}Cs	0.796	6.7
^{137}Cs	0.662	6.1456
^{58}Co	0.811	6.8
^{60}Co	1.173	8.1472
^{60}Co	1.332	8.7504

To compute the calibration factors for *in situ* soil counting for uniformly-distributed nuclides, the values given in Table 5-4E and Table 5-5E are substituted into Equation 3-1E.

The ϕ values from Table 5-5E are converted to ϕ/A by multiplying by the appropriate photon intensity. The calculation of the calibration factors is shown in Table 5-6E. The factors are given in terms of both cpm per Bq per gram (current convention) and cpm per μCi per gram.

Table 5-6E Calibration factors for in situ counting of uniformly-distributed sources ($\alpha/\rho = 0$) at a height of one meter

Nuclide	Energy	Intensity (γs^{-1} per Bq)	N_0/ϕ (cpm per g $cm^{-2} s^{-1}$)	N_f/N_0	ϕ (g cm^{-2})	Calibration Factor (cpm per Bq per gram)	Calibration Factor (cpm per μCi per gram)
^{134}Cs	0.569	0.1543	1.26E+03	1	5.7	1.11E+03	4.10E+07
^{208}Tl	0.583	0.842	1.25E+03	1	5.8	6.11E+03	2.26E+08
^{134}Cs	0.605	0.976	1.23E+03	1	5.9	7.11E+03	2.63E+08
^{214}Bi	0.609	0.463	1.23E+03	1	5.9	3.36E+03	1.24E+08
^{137}Cs	0.662	0.8512	1.19E+03	1	6.1456	6.20E+03	2.30E+08
^{134}Cs	0.796	0.854	1.09E+03	1	6.7	6.26E+03	2.32E+08
^{58}Co	0.811	0.994	1.08E+03	1	6.8	7.32E+03	2.71E+08
^{214}Bi	1.12	0.151	8.55E+02	1	8	1.03E+03	3.82E+07
^{60}Co	1.173	1	8.44E+02	1	8.1472	6.87E+03	2.54E+08
^{60}Co	1.332	1	6.77E+02	1	8.7504	5.92E+03	2.19E+08
^{40}K	1.461	0.1067	6.04E+02	1	9.1472	5.89E+02	2.18E+07

6. References

(EML 1990) Krey, P. W.; Beck, H. L. "EML Procedures Manual", 27th edition, Vol. 1, HASL-300, Environmental Measurements Laboratory, New York, NY, November, 1990.

(Helfer and Miller 1988) Helfer, I. K.; Miller, K. M. "Calibration Factors for Field Ge Detectors" *Health Physics*, Vol. 55, No. 1 (July), pp. 15-29, 1988.

(ICRU 1994) "Gamma-Ray Spectrometry in the Environment", ICRU Report 53, International Commission on Radiation Units and Measurements, Bethesda, MD, December 1, 1994.

Appendix F

SMCM Scan Survey Characteristics

1. Vehicle Speed Considerations

The SMCM software can trigger recording a spectrum of data for either a fixed time or for a fixed distance. For this survey, the data was triggered with a time based trigger set for ten-second intervals. The speed of the vehicle affects the meters that are traveled in ten seconds. At the desired pixel size of two meters, this corresponds to 0.2 meters per second (0.4 mph). In order to permit an operator to control a vehicle at that low speed, a specialized operator interface was developed. The user interface provided for the operator gave speed, time and distance traveled along a strip. In addition, indications were provided for speed required to complete the strip at the desired average speed. At times, the terrain made surveying quite difficult. Maneuvering the vehicle down a steep embankment could result in the ten-second acquisition averaging up to eight meters of travel. The field procedure was to obtain the correct average speed, and the operator would stop or travel more slowly for a few meters to maintain the proper average. The converse situation also occurs when the vehicle climbed up a steep stream bank or berm, resulting in less than two meters of travel in ten seconds. A screen capture of the user interface is shown in Figure 1-1F.

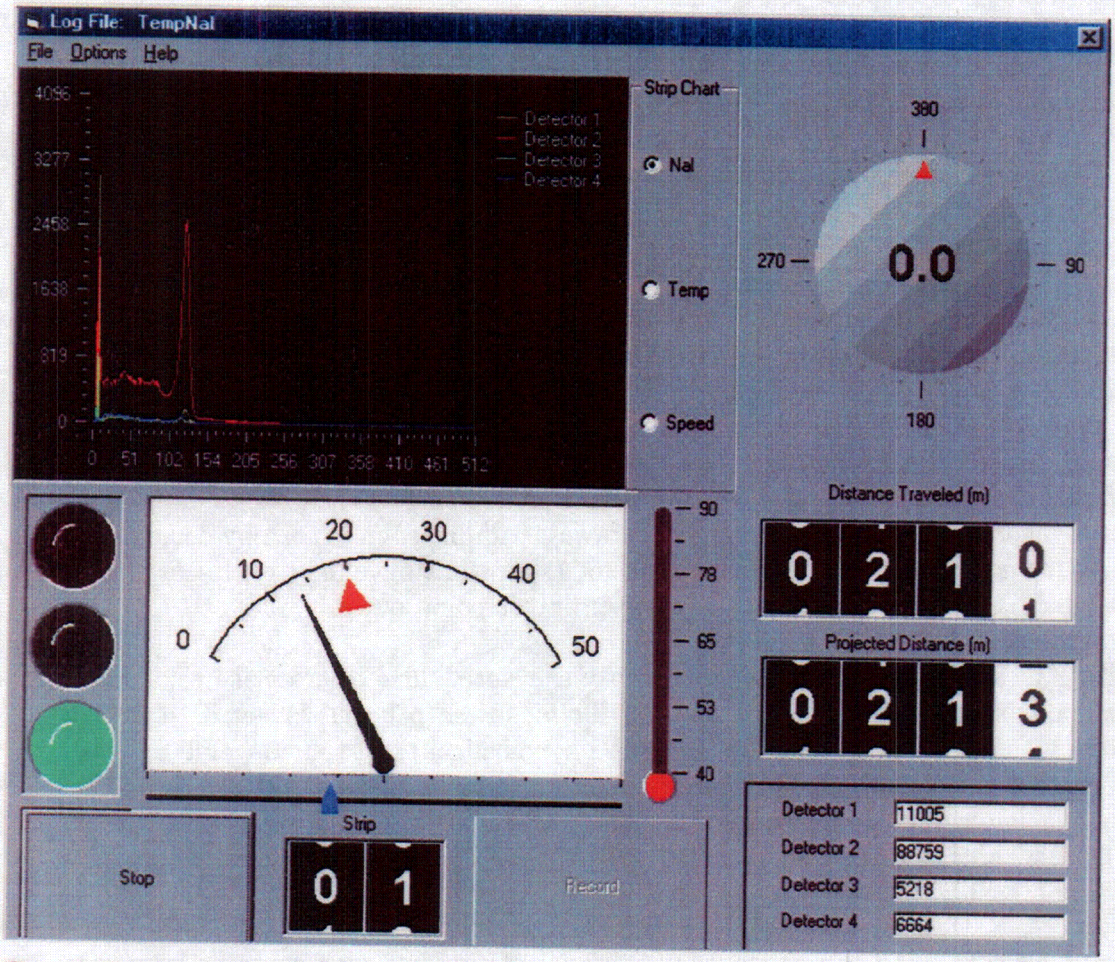

Figure1-1F– Screen capture of SMCM software user interface.

C12

As a result of the operator interface and training, the average speed in the average SAB was controlled such that the average for the entire survey was 2 meters with a standard error of less than one centimeter. Within the 300 measurements for an individual SAB, the standard deviation is larger, typically 70 centimeters. This means that the distance traveled corresponding to the ten-second acquisition was between 1.3 and 2.7 meters for 68% of the data. Four particularly difficult SABs had maximum length pixels that ranged between seven and ten meters in length.

The variation of the length of a pixel could affect the data in three ways: improper location designated for a real point source detected in the image; higher or lower detection limit for a hypothetical point source than computed using the assumption of constant speed; and blurring of a real point source in an image if adjoining pixels differ in size. The field of view of the detector is large, extending over tens of meters. Thus, there is little effect of varying pixel length on the detection or assessment of area average values. The dominant effect of varying vehicle speed is on point sources.

If there was a localized or point source that was detected, the location of the source could be slightly different than would be estimated using the assumption of a fixed pixel length. The distance traveled for each acquisition was recorded to allow estimating the position to find the source for follow up. As there were no point sources detected, this issue did not affect the survey results and reporting. However, to help show this phenomenon, a test grid with local position error is shown in Figure 1-2F. The bright pixels in the image are where the survey team "salted" the B1-3 grid with four ^{60}Co check sources with a total activity of about 1.6 μCi. Both pixels are from the same source placement. The one nearest the bottom corresponds to the SMCM traveling east-to-west with the sources seen by detector 1. The other pixel to the northeast of the first is also detector 1, but while traveling west-to-east. The shift of the row to the right is a result of this positioning error on a point source.

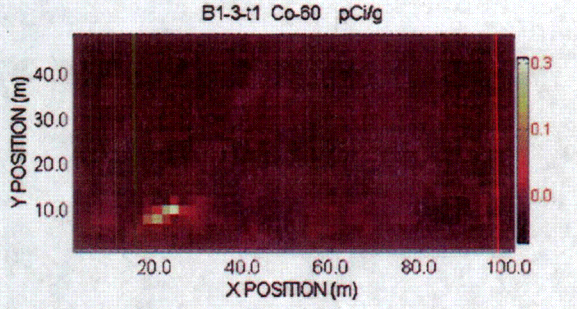

Figure 1-2F – Image plot of "salted" B1-3 test SAB displaying local positioning error.

If the vehicle is slowed to attain the correct average speed, the detector is resident over a hypothetical point source longer, and the detection limit is lower (better) than stated. If the vehicle is operated at higher speed, the detection limit for a hypothetical point source would be worse by the square root of the residence time (or speed). The four grids with largest distance traveled in ten seconds had maximum distances of between 7 and 10 meters, 3.5 to 5 times the nominal pixel size. Thus, the highest speed pixels, which occurred on 4 out of 66 grids, had a detection limit that was about a factor of two higher (worse) than stated.

The impact of vehicle speed was ignored as it did not affect large area source assessment. In addition, the speed adversely affected potential point sources on much less than one percent of the

nearly 80,000 measurements that were made. The detection limit was degraded by no more than a factor of two. As the detection limits that were attained by this survey were much better than a factor of ten times better than required, it is unlikely that any single measurement failed to attain a detection limit that met the performance requirement.

2. Detector Height Considerations

The detectors in the large array were subject to varying heights above the terrain. The height of the detectors could vary because of terrain variations, or because of roll or pitch motions on the vehicle.

The height dependence on pitch (vehicle oriented up or down from horizontal) was minimized by placing the array as close as possible to the front axle of the vehicle, which minimized the dependence of detector height on pitch. The dependence on roll (vehicle rotated left or right from horizontal) was greater. The inner detectors were one meter from the centerline of the vehicle and were less subject to height variation as a function of roll angle. The outer detectors were 3 meters from the centerline of the vehicle, and the front face of the detector was one meter above the terrain. They were in an enclosure, with the front of the enclosure at 92 centimeters above the ground. Thus, the outer detectors would contact the ground if the roll angle exceeded 17 degrees. To avoid damage and lost time, the operator prevented the detectors from contacting the ground by maneuvering the vehicle. However, at times, one of the outer two detectors came close (front face at 10 centimeters) to the ground, while the detector on the opposite side was lifted to a height of less than two meters.

The flux from a uniform source is constant as a function of detector height. The technical basis documents from the DOE Environmental Measurements Lab on *in situ* gamma spectroscopy state that the response function is nearly constant from one half meter to two meters (EML 1990). Thus, the impact on the survey from height variation with roll angle on large area sources is small and can be neglected.

The impact on small area sources can be estimated from the nearly inverse distance squared relationship of the detector to a point source. The detector near the ground has a substantial improvement in detection limit for small sources, perhaps as much as 100 fold. The detector that lifts away from the ground suffers a degradation of detection limit of a factor of 3.6. This was estimated to affect less than 10% of all of the measurements. In addition, as a result of the typical survey pattern (back and forth), the adjoining strip of data collected would reverse the travel over the ditch or obstacle and adjoining pixels in the next strip would be affected in the opposite manner as any affected pixel.

No point sources were detected. Thus, the impact on survey reporting was that the detection limit for point sources was worse than reported by a factor of from 2 to 4 on a small fraction of the nearly 80,000 spectra that were recorded. As the detection limits that were attained by this survey were much better than a factor of ten times better than required, it is unlikely that any single measurement failed to attain a detection limit that met the performance requirement.

Appendix G

Data Handling and Analysis Methods

The data from the SMCM for a given SAB consisted of 1200 each, 10-second spectra from the nominal 5X2 NaI(Tl) detectors. The energy range from 0 to 3 MeV was spanned with 512 channels. The data was converted to count rate, and adjusted by a factor that included the detector efficiency (relative to detector 1) and the platform shielding. This platform-shielding factor was applied to place the detectors on an equivalent response basis. This practice simplified the development of images from the data, and avoided "banding" in the image due to slight differences in response. It is mathematically equivalent to corrections applied to medical (gamma) cameras. The inner detectors were shielded from the ground by the frame, body and engine of the John Deere™ "Gator" platform. As a result, the count rate for naturally occurring radioactive potassium were slightly reduced. Two platform factors were used, one for the four detector array and one for the narrower three detector array that was used in the photovoltaic (PV) array field SABs.

The factor was determined in an iterative fashion. Raw data was examined in each of the energy windows in the gamma ray spectra that were studied, and the count rates for the two detectors mounted near the Gator were found to be systematically lower, on average, than the outer two detectors. The reduction was less than 10%, however, when uncorrected. This difference provides an image that is banded in appearance, since all of the pixels along a row of data are affected. Studies indicated that the factor was relatively insensitive to gamma energy, as the windows all had factors that were within two percent of each other. This lack of strong energy dependence can be explained in that most radiation interactions in this energy range are from the Compton scattering process. The Compton scattering cross section changes slowly with energy. Thus, a common factor was used for all windows for a given detector. At times, the data will appear to be slightly banded because of this simplification.

Following correction of the raw data by the platform-shielding factor, the spectra were analyzed and separated into components using the method of noise-adjusted single value decomposition (NASVD). (Hovgaard 1997). This is a statistical process that computes the spectral shapes that are embedded data. Following decomposition, the spectra are re-assembled without adding the noise back in. This process reduces the noise by a factor of 4 or more, and improves the signal to noise by more than a factor of two. The same gain in signal to noise would require counting four times as long. This means each 10 second spectra was equivalent to 40 seconds of counting (if the NASVD method was not used). The typical SAB had 1200 such acquisitions. The larger detectors (5x2) are about 2.5 times more efficient than the (3x3) detectors often used for *in situ* measurements.

Another significant advantage of NASVD is that the components that are present are presented as separated spectra. If any nuclides of concern were present at detectable levels, the spectral shape from these nuclides would be observed in the components. Following the NASVD, the components were examined for any sign of ^{134}Cs, ^{137}Cs or ^{60}Co. This provides the most sensitive signal for demonstrating that the site is indistinguishable from background. Two SABs were measured as a performance test of the system. These included an SAB that was repeated with a few small button check source intentionally left in the field, and an area of the site that was known to be contaminated with ^{137}Cs from past operations. Both of these SABs provided strong signals for ^{137}Cs and for ^{60}Co. The ^{60}Co signal was present even when detector 1 was removed from B1-3T1 (corresponding to the bright spots shown in Appendix F, Figure 1-2F). Thus, a signature for ^{60}Co was obtained from the other three detectors as well.

The spectra were then reconstructed, and potassium, uranium and thorium net windows were calculated using methodology developed by the IAEA. (IAEA 1979). In addition, windows were extracted corresponding to the energies of the nuclides of concern (^{134}Cs, ^{137}Cs, and ^{60}Co). Windows corresponding to a high energy gross count rate and to the count rate in a low energy Compton window were also computed. The windows for the nuclides of concern were then corrected for the effect of terrain, using a terrain factor.

The terrain-shielding factor accounts for the fact that a detector in a ditch will have higher count rates that on a flat earth (which is the assumed geometry for the conversion factor from count rate to concentration). A detector on the peak of a hill will have a lower count rate. On any given grid, the rolling terrain and ditches caused the window count rate data for the nuclides of concern to have to have a large standard deviation. This can be reduced for examining each SAB for differences from background.

The terrain factor was measured using the potassium window data, and applied to the data for the nuclides of concern. The validity of the terrain-shielding factor relies on several assumptions. If the count rate from the nuclides of concern is low compared to background, most of the counts will be due the primordial nuclides potassium, uranium, and thorium (KUT). Under these conditions, the count rates for the windows of the nuclides of concern will be correlated with the primordial (IAEA) windows. The component data for all grids was analyzed, and no evidence was found for peaks that could be attributed to the nuclides of concern. The data also showed that the uranium and thorium were low as compared to potassium and the ratio of K:U and K:T was broadly similar from SAB to SAB. Finally, the windows for the nuclides of concern were found to have correlation constants between 0.7 and 0.9 (highly correlated) with the count rate for potassium. Thus, the requirements for applying the terrain factor were satisfied.

The terrain factor uses the local variability of the potassium within a grid as a measure of the terrain. A ratio was created that was the average site potassium count rate divided by the potassium measurement for a given pixel. The ratio typically was between 0.5 and 2. Within an SAB, 0.5% of the data for either the maximum factor or minimum factor was capped at the 0.5% (or 99.5%) level. This was done to avoid using a terrain factor that had statistical extremes. If the potassium window count rate was adjusted by the factor, a constant value of count rate equal to the site average would have resulted for all potassium measurements within the SAB. When multiplied by the window data for the nuclides of concern, the local variability, as measured by the standard deviation of the data within an SAB was reduced. The reduction was not noticeable for poorly correlated SABs, but was more than a factor two for SABs that had highly variable terrain (and potassium measurements).

The terrain factor greatly reduced the standard deviation of the data for the nuclides of concern, and thus reduced the implied limit of detection calculated using the 1200 measurements. In grids that were affected by terrain, the standard deviation of the ^{137}Cs window, for example, dropped from the 15% to 20% range to the 5% to 10% range. On grids that were unaffected by terrain, there was a slight increase in the standard deviation. The terrain factor removes the variability and correlation with KUT, but does not change the average count rate for a given grid. Thus, calculation of the limit of detection remains valid (see Volume II, SMCM Data Tables for more detail).

If ^{137}Cs was actually present, use of a terrain factor would improperly scale the net value for concentration, as the window is not correlated to potassium when the ^{137}Cs count rate dominates. This did not occur for the survey area. It does occur in the two SABs that were used to test the performance of the system.

Following application of the terrain factor, the data was assembled into spatial data sets using the Survey Information Management System (SIMS) and was filtered using a Weiner filter (NUREG/CR-6450). For the nuclides of concern, a site wide average value was then determined and subtracted from all data to obtain net count rate, which was converted into equivalent concentration on pCi/g.

Appendix H

Comparison of SAB Means via Statistical Tests

The Rancho Seco Non-Industrial Area Radiological Survey Project was performed for the purpose of characterizing background in the non-industrial areas of the site and to identify any areas where there was plant-related residual radioactivity that was distinguishable from background. Such a comprehensive effort does not lend itself to evaluation using the simple nonparametric statistical tests described in the MARSSIM for final status surveys in that the survey objectives were very different than those for a final status survey. If a comparison against the radiological criteria for license termination prescribed in 10 CFR 20 subpart E was desired for the areas surveyed, this would be a trivial exercise given the completeness of the survey effort. The MARSSIM statistical tests would not be needed to demonstrate that the various SABs met the criteria of subpart E.

The MARSSIM nonparametric statistical tests are prescribed assuming a survey modality where the number of measurements made in an individual survey unit is not large (less than 30 or so). Thus, these tests are of limited use in a case where a survey method such as the one used in this project is employed. The number of measurements is so large there is no need for nonparametric evaluations such as those described in NUREG-1505, and by extension, the MARSSIM. Instead, the comparison of the survey results against the applicable criteria can be achieved through inspection.

In the case where the goal of a survey is to demonstrate that an area does not contain residual activity that is distinguishable from background, it is desirable to use a statistical approach where this is the null hypothesis being tested. Such an approach is the opposite of what is used in the MARSSIM to demonstrate compliance with the radiological criteria for license termination specified in 10 CFR 20 subpart E. In the case of license termination surveys, the null hypothesis being tested is that a survey unit contains activity in excess of the $DCGL_W$. The goal of the survey is to collect an adequate amount data to either accept or reject this hypothesis with acceptable statistical confidence. Testing against this null hypothesis is more straightforward than testing for distinguishability from background in that there are fewer assumptions and statistical tests involved. The reason such an approach can be applied is that the difference between the applicable $DCGL_W$ and background is assumed to be large enough where adequate statistical power can be achieved with a relatively small number of measurements. However, in cases where variability in background cannot be ignored, testing a null hypothesis that an area contains residual activity in excess of a release criteria can result in unacceptable decision error rates. It is therefore preferable in such cases to test a null where the area does not contain activity distinguishable from background.

The appropriate statistical test to use to demonstrate that two samples are not statistically distinguishable depends on knowledge about the true distributions of the population means being compared (even if nonparametric methods are to be employed) and the number of samples available. NUREG-1505 describes a nonparametric method of demonstrating indistinguishability from background where the survey protocols described in the MARSSIM are employed to compare an area of interest to a reference area. The method is essentially a three part approach where one first determines if there is significant variability (relative to the applicable $DCGL_W$) among the available reference areas. This is done using a nonparametric analysis of variance technique known as a Kruskal-Wallis test. If the Kruskal-Wallis test shows that there is variability among reference areas beyond that expected from statistical variability alone, the magnitude of this variability

(quantified by the component of variance that is not accounted for by statistical variability) is determined. Comparisons between areas under consideration and the reference areas to determine if the area contains activity that is distinguishable from background are then performed using a Wilcoxon Rank Sum test, with the lower bound of the gray region (LBGR) set to the concentration above background that may be considered distinguishable. The null hypothesis being tested is then that the difference between the median concentration in the survey area and that in the reference area is less then the LBGR.

While the method described in NUREG-1505 for demonstrating indistinguishability from background would result in lower decision error rates than if the null hypothesis being tested was that the survey area contained distinguishable activity, it still relies on a survey modality where a relatively small number of measurements are made in the reference areas and the areas under consideration. Thus, this method is impractical as a means to compare the results from the Rancho Seco background characterization survey in that there was an enormous number of measurements made over a large area of the site. Statistical comparisons based on acquiring a few measurements in just a few areas do not make sense here.

Rather than rely on nonparametric analysis methods intended for small sample sizes, the Rancho Seco data were examined using a traditional parametric method of comparing sample means. Means results from various SAB were compared to demonstrate that these results were statistically indistinguishable at levels equivalent to small fractions of their combined variability (precision). SABs selected for comparison were not chosen randomly, but were instead chosen based on their relative proximity to show that the results for SABs that were spatially close together were no different than those for SABs that would have shown distinguishability if they had been affected by plant operations. A simple parametric assessment could be used since the large amount of data allowed the assumption of normal (Gaussian) behavior to be verified.

SABs were compared by determining the difference between the two mean values of interest where the value of the t-statistic for the two data sets equaled the critical value for a given significance level and for the degrees of freedom for the two data sets combined. This is the equivalent of determining the additional dispersion (imprecision) that must be added to the difference of the two sample means so that they can no longer be statistically distinguished. This approach had to be used instead of a traditional t-test (where the null hypothesis is that the means are equal) since the large number of measurements in each SAB resulted in very small dispersions about each mean. As a result, all of the SAB means are statistically distinct since their associated standard deviations are so small. The general expression for computing test value for the t-statistic is shown in the following equation:

$$T_v = \frac{\left|\overline{Y}_1 - \overline{Y}_2\right| - \delta}{\sqrt{\frac{s_1^2}{N_1} + \frac{s_2^2}{N_2}}} \qquad \textit{(1-1H)}$$

where: T_v = test value of the t-statistic for v degrees of freedom given by the sample variances and the number of measurements in each sample;

$\bar{Y}_1$ = value of the first sample mean of interest;
$\bar{Y}_2$ = value of the second sample mean of interest;
δ = additional difference (imprecision) between the two means;
s_1^2 = sample variance for the first sample mean of interest;
s_2^2 = sample variance for the second sample mean of interest;
N_1 = number of measurements in the first data set; and
N_2 = number of measurements in the second data set.

The expression for computing the additional imprecision that must be added to the difference in sample means is shown in Equation 1-2H.

$$\delta = -\left[t_{\alpha,\nu} \sqrt{\frac{s_1^2}{N_1} + \frac{s_2^2}{N_2}} - \left| \bar{Y}_1 - \bar{Y}_2 \right| \right] \qquad (1\text{-}2H)$$

where: $t_{\alpha,\nu}$ = percentile value for Student's t-distribution for significance level α and degrees of freedom (ν).

Degrees of freedom for the t-statistic were estimated assuming that the sample variances were not equal. This was a formality, however, since the large number of measurements made in each SAB made precise estimation of ν unnecessary. With such large numbers of measurements, the t-distribution is equivalent to the normal distribution. All of the comparisons were performed at a significance level of 0.05, corresponding to a 95% confidence level. SABs were compared on the basis of the mean count rates for the ^{137}Cs, ^{40}K and uranium windows. ^{40}K was chosen as a proxy for spatial variability of background since it has the highest count rates of the three primordial nuclide windows and since the relative proportions of the three primordial constituents are reasonably constant over the site. ^{137}Cs was chosen as the best indicator of plant-related residual radioactivity, and the uranium window was used as an indicator of the variability in airborne radon concentrations. Both the spatial variability of the background and the temporal variability of airborne radon affect the ^{137}Cs window.

To provide a basis for assessing the effect of the temporal variability in airborne radon concentrations, a comparison was made between two sets of survey results for SAB B1-3. This area was surveyed on two different occasions 8 days apart to confirm that there was not any significant variability in the overall survey method. The comparison of the results from the two surveys are summarized in Table 1-1H below. Comparisons were made for all energy windows of interest.

Table 1-1H Comparison between two surveys performed for SAB B1-3

Energy Window	First Scan (12/4/2000)		Second Scan (12/12/2000)			
	mean (cps)	variance (cps)	mean (cps)	variance (cps)	difference	δ (cps)
^{137}Cs	14.54	1.66	13.11	1.59	-9.8%	1.34
^{134}Cs	7.85	0.55	6.98	0.55	-11.1%	0.82
^{60}Co	6.68	0.39	5.75	0.36	-13.9%	0.89
^{40}K	4.43	0.27	4.36	0.29	-1.7%	0.03
Uranium	1.30	0.03	0.84	0.02	-35.6%	0.45
Thorium	1.51	0.03	1.46	0.04	-3.9%	0.04
Gross	79.29	45.35	71.15	47.48	-10.3%	7.68

In Table 1-1H, each pair of mean values is statistically distinct. The δ value is the additional difference in the means that would have to be added before for them to become statistically indistinguishable. Note that the data used in these comparisons (gross count rates) differ from what is used elsewhere in this report. The data used in the comparison of SAB means have only been corrected for the effect of the survey platform and for efficiency (normalized to Detector 1). The only other correction applied was application of the IAEA stripping coefficients to the energy windows for the three primordial series. Comparison of the SAB means is not as sensitive a technique as the other data analysis methods used in this report since the ability to discern differences in two data sets is affected by the variance of both sets. Data analyses that consider the SABs individually thus provide better sensitivity. Such evaluations are affected by only the variability within a single SAB, rather than the combined effects of the variability within two blocks plus that across them. One should also note that since the comparisons performed in this section utilize gross rather than net data, the δ-values should not be compared directly with the net pCi/g values reported elsewhere in this report. The δ-values are intended to be compared relative to one another.

Comparing the results between the two surveys for SAB B1-3 shows a significant decrease in the apparent uranium concentration. The fact this decrease is not seen for the other primordial nuclide windows (^{40}K and ^{232}Th) indicates that this difference is due to a difference in the airborne radon concentration between the two surveys. The first survey was performed between approximately 9:00 am and 10:00 am on December 4, 2000 and the second survey was performed between approximately 2:00 pm and 3:00 pm on December 12, 2000. The different times of the day for the two surveys are therefore consistent with the phenomena of diurnal variability in airborne radon concentrations, though there could be other contributing factors (e.g., rainfall).

The results for the ^{137}Cs, ^{134}Cs, ^{60}Co and gross count windows all show the effect of the lower apparent uranium concentration, with the magnitude of the effect decreasing with decreasing energy. The ^{40}K window does not show the effect of the reduced downscatter continuum between the two surveys because this energy region has had the IAEA stripping coefficient applied. The effect of the reduced apparent uranium concentration has therefore been removed. Thus, the ^{137}Cs, ^{134}Cs and ^{60}Co windows are sensitive to diurnal variability in airborne radon concentrations where the ^{40}K window is not. The ^{40}K and ^{232}Th windows are therefore good indicators to use

to check for systematic bias between the surveys. Comparing the results for these two windows for the two surveys shows no appreciable difference vis-à-vis that would reasonably be expected for field measurements.

The results of the comparison between the two surveys performed for SAB B1-3 can be used as a reference when comparing results between different SABs that were surveyed at different times. However, the comparison of the survey results for SAB B1-3 show this effect to be small relative to significant concentrations of ^{137}Cs.

A second approach to assessing at what point a difference in mean concentrations (characterized by the δ value) becomes large enough to suggest the presence of non-background radioactivity is to compare survey results for SABs that are spatially close together that should not have been impacted substantially by temporal variability in airborne radon concentration. This approach provides an indication of expected variability between means from different SABs that is due to spatial variability in background. Comparisons were made for SABs D3-1, D3-2 and D3-3 since these areas were all adjacent to one another and were surveyed in chronological order on the afternoon of December 10, 2000. These comparisons are summarized in Table 1-2H below.

Table 1-2H Comparison between SABs D3-1, D3-2 and D3-3

	SAB D3-1		SAB D3-2		SAB D3-3	
Energy Window	Mean (cps)	Variance (cps)	Mean (cps)	Variance (cps)	Mean (cps)	Variance (cps)
Cs-137	13.36	0.42	13.04	0.42	14.55	1.06
K-40	5.49	0.14	5.55	0.12	5.66	0.37
Uranium	0.91	0.03	0.94	0.02	0.96	0.03
δ-value for Cs-137 D3-1 vs. D3-2 = 0.28 cps						
δ-value for Cs-137 D3-2 vs. D3-3 = 1.45 cps						
δ-value for Cs-137 D3-1 vs. D3-3 = 1.13 cps						

The comparison of SABs D3-1, D3-2 and D3-3 provides an idea of the magnitude of the spatial variability of SAB means for the ^{137}Cs window independent of the effect of differences in airborne radon concentration. This variability is seen to be on the same order as that from radon variability, and thus is also a small effect relative to significant concentrations of ^{137}Cs.

Having compared SABs for the purpose of assessing the magnitude of the effects of spatial and temporal variability of background, three pairs of SABs were then selected for comparison on the basis of their potential for having been affected by plant operations. SABs were selected to see if any of the following distinctions could be drawn using the ^{137}Cs data:

- higher concentration in the prevailing wind direction than in the cross-wind direction;
- higher concentration closer to the plant than farther away (in line with the prevailing wind);
- higher concentration in low-lying areas than in higher areas.

The two SABs selected for the prevailing wind – cross-wind comparison were D1-4 (prevailing wind) and A1-2 (cross-wind). The SABs chosen for close to the plant were E2-4 (near) and F1-5 (far), and those chosen for higher elevation versus lower were E2-1 (high) and C1-3 (low). The ^{137}Cs window data for these six SABs are summarized in Table 1-3H below.

Table 1-3H Cs-137 window data for selected SABs

SAB Number	Mean (cps)	Variance (cps)
D1-4	13.95	1.67
A1-2	17.34	1.09
E2-4	12.56	0.70
F1-5	13.23	0.94
E2-1	13.94	0.50
C1-3	13.38	1.94

The δ-values for the ^{137}Cs window for each pair of SABs are given in table 1-4H below.

Table 1-4H Cs-137 δ-values for selected SABs

Comparison	Cs-137 δ-value (cps)
D1-4 vs. A1-2	3.31
E2-4 vs. F1-5	0.60
E2-1 vs. C1-3	0.48

The comparison for the near vs. far and high vs. low areas clearly do not suggest any evidence of plant-related radioactivity. The δ-value for the prevailing wind versus cross-wind is somewhat higher than those observed in the comparison of SABs for the effect of spatial or temporal variability independently, but is consistent with a combined effect from these two phenomena.

Appendix I

Performance-Based Test Survey

In addition to the 62 SABs included within the scope of the survey project, SRA also conducted a field test survey aimed at providing measured performance information for the SMCM. An SAB with the same 48 meter by 100 meter dimensions was placed within the effluents discharge area southwest of the Industrial Area known to have plant-borne contamination. This location was chosen for two reasons: the presence of actual contamination provided a real "measuring stick" for determining the areal detection limits of the SMCM; and Rancho Seco radiological staff had already performed an extensive exposure rate survey of the area for comparison against the SMCM results. The results of the exposure rate survey are shown in Figure 1-1I. The chosen location for the SAB was between the B1 and B3 Survey Areas defined in Section II near the orange "Y" artifact at the intersection of rows AI and AJ and columns 11 and 12. The new SAB was named B5-1.

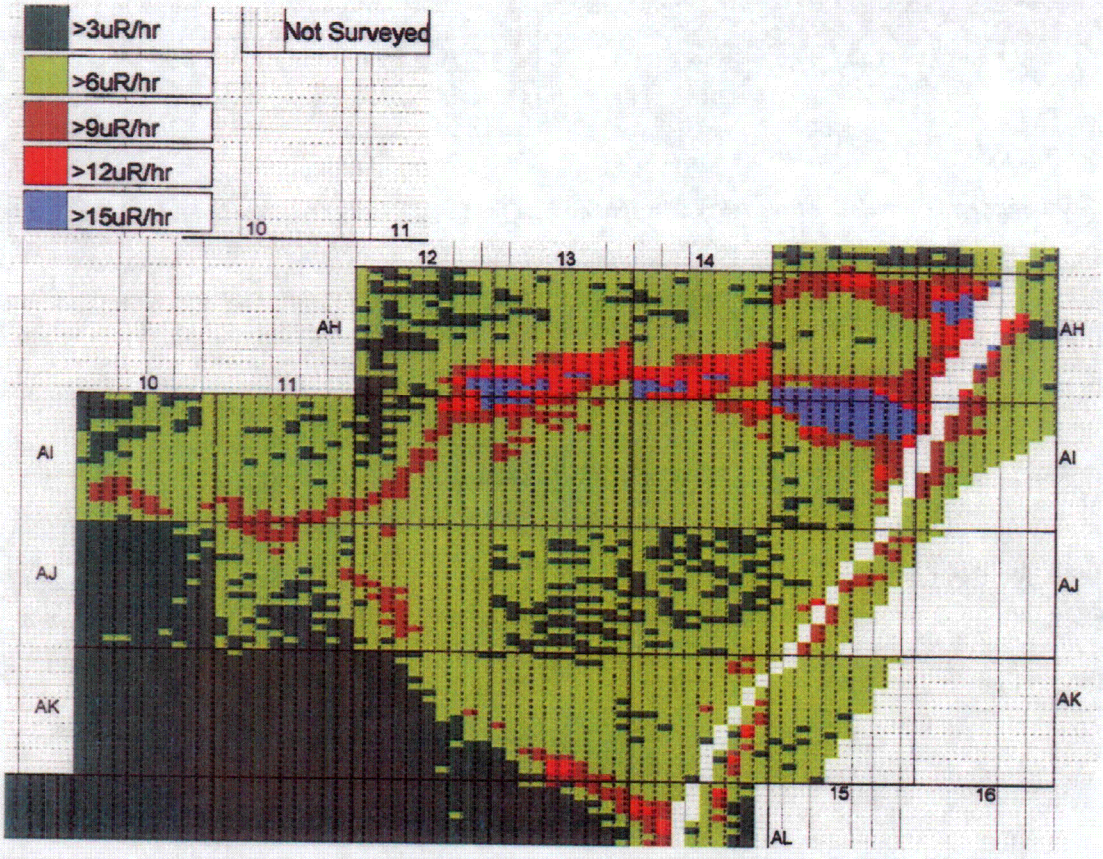

Figure 1-1I - Image of exposure rate survey performed for effluents discharge area.

This data recorded the maximum micro-R per hour readings in a 5-foot by 10 foot area with the instrument set with a long time constant. Backgrounds appear to be in the 4-7 μR/hr region, and areas in excess of 10 μR/hr likely contaminated.

The results of the scan survey for B5-1 are shown in Figure 1-2I. The extent of the ^{137}Cs contamination is easily seen in the data. The "Y" artifact shown in Figure is also seen here but in far greater detail. The color threshold has been auto-scaled to the lowest pixel value to bring out the contrast in the image. The contrast is also highlighted in the CFD plot, with the ^{137}Cs in the

"Y" shown as the near-horizontal line. The steep slope of the line near the origin of the CFD indicates those pixels surrounding the "Y" that are closer to background levels. The x-axis of the CFD indicates that the departure from background for B5-1 occurs at levels less than 1 pCi/g.

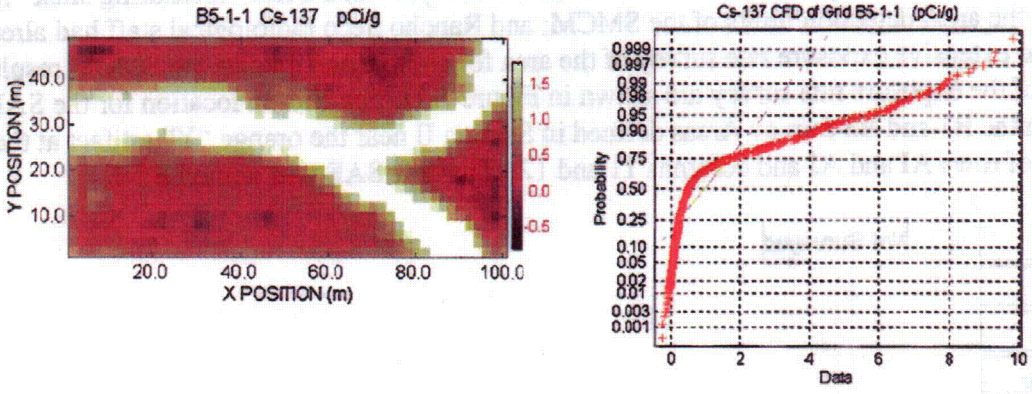

Figure 1-2I – 2-D Image and Cumulative Frequency Distribution Plot for Cs-137 energy window in SAB B5-1.

To test the sensitivity of this imaging process, this measured ^{137}Cs contamination was used in conjunction with the data from "clean" SABs to determine at what levels could the SMCM positively identify distributed sources of ^{137}Cs. First, the elevated "Y" region of SAB B5-1 was subtracted from the baseline levels in the area surrounding the "Y" to create a residual ^{137}Cs signature. This residual matrix then is superimposed on the 2-D image from another SAB at varying levels of intensity until the "Y" can no longer be distinguished from the background levels in the Cs energy window in that SAB.

The SAB used for the residual addition test was A1-7 as it was determined to have the highest background in the ^{137}Cs window, on the Rancho Seco site, corresponding to 1.28 pCi/g. The choice of the highest background grid was intentional as it serves as the limiting case for the effectiveness of this method. Figure 1-3I shows the results of the residual addition to SAB A1-7. Shown are 100%, 25%, 10%, and 5% of the residual matrix added to the same image.

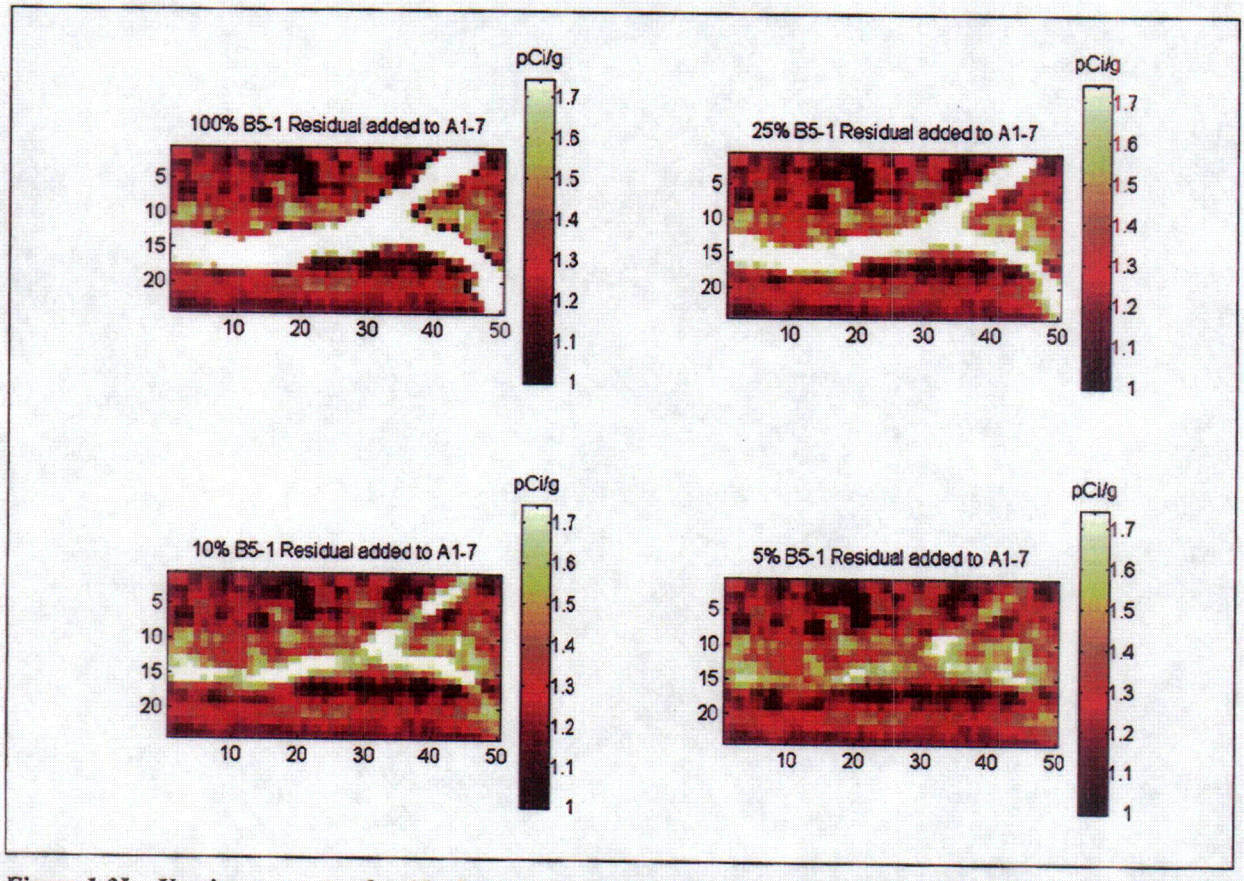

Figure I-3I – Varying amounts of residual contamination from SAB B5-1 added to SAB A1-7 to identify threshold values for visual identification.

As the level of residual decreases, the definition of the "Y" in the image fades to the point where the structure virtually disappears (see 5%). However, at 10%, the structure of the "Y" is still visually apparent in the image, corresponding to a net ^{137}Cs addition between 0.5 – 0.9 pCi/g based on the measured values for B5-1. Naturally, this threshold would be substantially lower for areas with lower backgrounds as the relationship scales proportionately. For example, it is likely that less than 5% of the residual B5-1 matrix would easily be identified in the D1 and D3 Survey Areas as these had extremely low ^{137}Cs background levels.

The average ^{137}Cs level measured in the test grid was 1.3 pCi/g. Taking credit for a factor of 10 reduction as shown from the worst grid above means that this method could detect ^{137}Cs at levels up to 100 times lower than the guidance levels present in the Federal Register.

C1G

Appendix J

Source Calibration Certificates

CERTIFICATE OF CALIBRATION
GAMMA STANDARD SOURCE

Radionuclide:	Cs-137	Customer:	MILLENNIUM SERVICES, INC.
Half Life:	30.17 ± 0.16 years	P.O. No:	98-1003
Catalog No.:	GF-137	Reference Date:	1 Jul 98 12:00 PST
Source No.:	619-38-1	Contained Radioactivity:	9.301 μCi
		Contained Radioactivity:	344.1 kBq

Source Description

a. Capsule type:	D
b. Nature of active deposit:	Evaporated metallic salt
c. Active diameter/volume:	5 mm
d. Backing:	Epoxy
e. Cover:	Acrylic

Radioimpurities:

None detected

Method of Calibration

This source was assayed by gamma spectrometry:

Energy peak(s) integrated under:	662	keV.
Branching ratio(s) used:	0.851	gamma rays per decay.

Uncertainty of Measurement

a. Systematic uncertainty in instrument calibration:	± 3.0%
b. Random uncertainty in assay:	± 0.8%
c. Random uncertainty in weighing(s):	± 0.0%
d. Total uncertainty at the 99% confidence level:	± 3.1%

NIST Traceability

This calibration is traceable to the National Institute of Standards and Technology.

Leak Test(s)

See reverse side for Leak Test(s) applied to this source.

Notes

1. IPL participates in an NIST measurement assurance program to establish and maintain implicit traceability for a number of nuclides, based on the blind assay (and later NIST certification) of Standard Reference Materials (As in NRC Regulatory Guide 4.15).

QUALITY CONTROL

18 Jun 98
Date Signed

ISOTOPE PRODUCTS LABORATORIES
1800 N. KEYSTONE STREET
BURBANK, CALIFORNIA 91504
818•843•7000 FAX 818•843•6168

IPL Ref. No.: 619-38

CERTIFICATE OF CALIBRATION
GAMMA STANDARD SOURCE

Radionuclide:	Co-60	**Customer:**	MILLENNIUM SERVICES, INC.
Half Life:	5.271 ± 0.001 years	**P.O. No:**	98-1003
Catalog No.:	GF-060	**Reference Date:**	1 Jul 98 12:00 PST
Source No.:	578-32-17	**Contained Radioactivity:**	0.8029 μCi
		Contained Radioactivity:	29.71 kBq

Source Description

a. Capsule type:	D
b. Nature of active deposit:	Evaporated metallic salt
c. Active diameter/volume:	5 mm
d. Backing:	Epoxy
e. Cover:	Acrylic

Radioimpurities:

None detected

Method of Calibration

This source was assayed by gamma spectrometry:

Energy peak(s) integrated under:	1173, 1333	keV.
Branching ratio(s) used:	0.9986, 0.9998	gamma rays per decay.

Uncertainty of Measurement

a. Systematic uncertainty in instrument calibration:	± 3.0%
b. Random uncertainty in assay:	± 1.9%
c. Random uncertainty in weighing(s):	± 0.0%
d. Total uncertainty at the 99% confidence level:	± 3.6%

NIST Traceability

This calibration is traceable to the National Institute of Standards and Technology.

Leak Test(s)

See reverse side for Leak Test(s) applied to this source.

Notes

1. IPL participates in an NIST measurement assurance program to establish and maintain implicit traceability for a number of nuclides, based on the blind assay (and later NIST certification) of Standard Reference Materials (As in NRC Regulatory Guide 4.15).

QUALITY CONTROL

18 Jun 98
Date Signed

ISOTOPE PRODUCTS LABORATORIES
1800 N. KEYSTONE STREET
BURBANK, CALIFORNIA 91504
818•843•7000 FAX 818•843•6168

IPL Ref. No.: 578-32